Lund University
&
Forschungszentrum Telekommunikation Wien

Modeling Spatial Interference for Multiple Users in MIMO Channels

Zhinan Xu

Supervisor: Nicolai Czink
Examiner: Fredrik Tufvesson

August, 2011

Acknowledgment

I would like to thank those people who helped me with my master thesis work in the past seven months. To begin with, I would like to thank Dr. Nicolai Czink and Dr. Thomas Zemen at FTW, Austria for providing me the opportunity to work on this exciting project. I also want to thank Dr. Fredrik Tufvesson for his recommendation and kindly providing supervision in Lund.

During the entire course of this thesis work, I would like to express my sincere gratitude to my supervisor Dr. Nicolai Czink, for his guidance, good research ideas, always being available for discussions and helping me exploit various possibilities in my work. Furthermore, I would like to thank MSc. Fernando Sanchez, MSc. Mingming Gan and Dr. Bernd Bandemer for their discussions and help.

Last but not least, I also want to thank my parents for their love.

The past two years have been very special experience. The student life in Lund and in Vienna will always be a valuable memory for me.

Zhinan Xu
August 30, 2011

Abstract

For an interference-impaired multiple-input multiple-output (MIMO) channel, the severity of the interference is not only determined by the power ratio between intended signal and interference, but also by the degree of alignment between the eigenspaces of the their channel matrices. The focus of this thesis is to study the spatial compatibility by means of the channel receiver correlation matrices.

First, the multi-user MIMO channel model is reviewed. We parameterize the multi-user MIMO channel model from real radio measurements. Several distinct distributions of spatial compatibility between intended and interfering transmissions are found for different types of movement. I evaluate and parameterize the multi-user MIMO channel model from the aspect of mutual information increase by providing the relationship between the eigenvalue structures of the receiver correlation matrices and the increase of mutual information. Furthermore, I evaluate and parameterize the model under interference from multiple users and find how the mutual information is affected by the eigenspace similarity between them.

To better use the spatial resources, I propose a user grouping scheme for uplink multi-access channels using the newly-developed mutual information metric. Simulations show that this grouping scheme offers a gain in spectral efficiency and system throughput due to more efficient use of spatial resources.

Contents

List of Figures

CHAPTER 1

Introduction

This chapter gives an introduction of this thesis. Firstly, I introduce the technical context of cooperative communication. The motivation of modeling spatial interference and interference scheduling techniques are given in Section 1.2 and Section 1.3. Section 1.4 describes related previous work. Finally, the contributions are presented in Section 1.5.

1.1 Background

Multiple-input multiple-output (MIMO) communications is an advanced technique to significantly increase the channel capacity, spectral efficiency, and transmission reliability by exploiting the spatial domain of fading channels [1], [2]. It has been shown to yield remarkable capacity, which increases linearly with the minimum number of antennas at the transmitter and receiver [3]. It also has been widely known that certain transmit diversity techniques (i.e., Alamouti scheme [4]) have been proposed into wireless standards, which improve the reliability of data transmission.

Cooperative communications [5] aims to utilize distributed antennas on multiple radio devices to reap some benefits similar to those provided by traditional MIMO techniques. The basic idea of cooperative MIMO is to form a virtual antenna array by grouping multiple nodes in a wireless network without each node necessarily having multiple antennas. The mobile wireless channel suffers from fading, which means that the attenuation of signal may vary significantly over the process of a given transmission. Transmitting independent faded copies of the same information through different paths can effectively combat effects of fading.

In the context of cooperative communication, the cooperative behavior

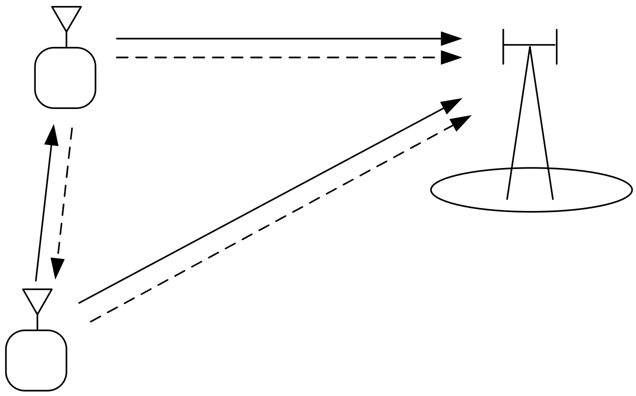

Figure 1.1: Cooperative communication

is exhibited as nodes mutually helping each other, as illustrated in Fig. 1.1. All involved nodes have their own data to transmit and mutually try to get it successfully delivered.

Cooperative MIMO systems have shown the advantages that without any extra cost resulting from the deployment of a new infrastructure and by using the existing resources of the network, it promises increased capacity, enhanced connectivity, improved performance in terms of path loss, diversity, multiplexing gains, and better quality of service together with a larger coverage range. However, it is indeed very important to realize that it is nearly impossible to develop a system without any imperfection. In the same way, cooperative systems come together with several challenges. Among them, the increase of interference is worth notice [6].

It is the radio channel, which ultimately determines the possible performance of such systems. Thus, the knowledge of its behavior is important for algorithm and system design. For the purpose of accurately assessing and comparing the performance of different interference management techniques for cooperative MIMO systems, realistic multi-user MIMO channel models are of great importance.

1.2 Motivation

Let us consider the n-user MIMO interference channel shown in Fig. 1.2, with n transmit-receive pairs. A wireless channel connects each receiver to each transmitter. However, for a given transmitter, its signal is only intended to be received and decoded by a single receiver. At the receiver, each link, including all intended and interfering links, is associated with a receive correlation matrix.

Correlated MIMO channels have been theoretically studied mainly using

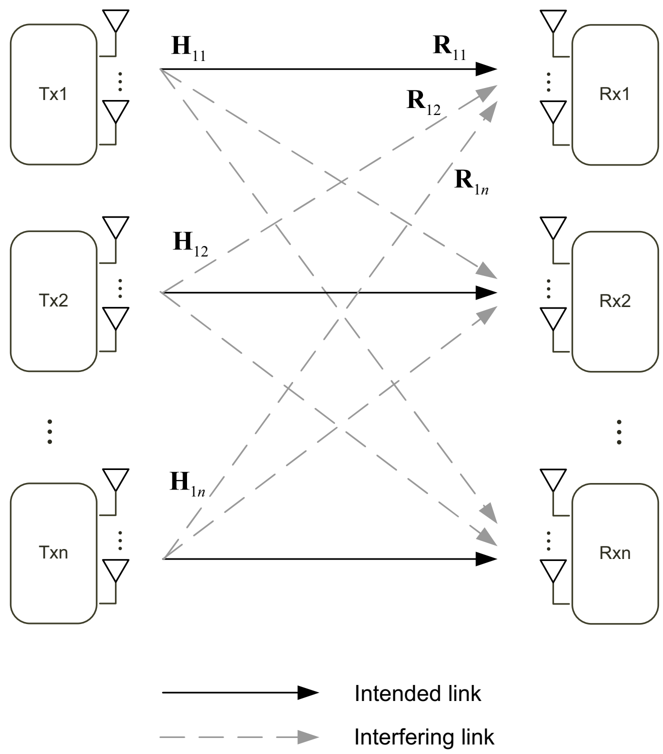

Figure 1.2: Multi-user MIMO interfering channels

the well known Kronecker model [7]. It assumes separability of the full correlation matrix into the transmit and the receive correlation matrix. This limits the degrees of freedom in modeling the channel, and also the accuracy of the model.

If the transmitters are in close vicinity of each other, where the distance between transmitters is significantly smaller than the distance from transmitter to receiver, the respective receive correlation matrices will be similar. On the other hand, if the distance between transmitters is far away, which is comparable to distance from transmitter to receiver, the channels will exhibit distinctive receive correlation matrices. In the ideal case that the correlation matrices are orthogonal, and thus signals do not live in the same subspaces, data can be transmitted simultaneously without interfering with each other. In reality, the signal subspaces overlap in most cases and no interference-free transmission can be guaranteed. The degree of subspace alignment is a vital factor in determining the capacity of interference-impaired channel.

An interference-impaired channel model, which is able to capture the behavior of subspaces (i.e., the transition from perfect orthogonal to fully overlapped), has been proposed by Czink et al. [8]. In this model, users are allowed to choose the severity of interference that they want to simulate, by selecting not only the signal to interference power ratio, but also by the degree of subspace alignment.

1.3 Interference scheduling

In this thesis, a spatial scheduling scheme is designed to leverage gains in spectral efficiency and system throughput. Besides the spatial domain, interference control also needs to be performed in time, frequency, or in code domain. Appropriate multiple access protocols are required in the presence of more than one user or at least one relay in the system, otherwise interference between multiple access users will occur. As depicted in Fig. 1.3, there are following channel configurations [6].

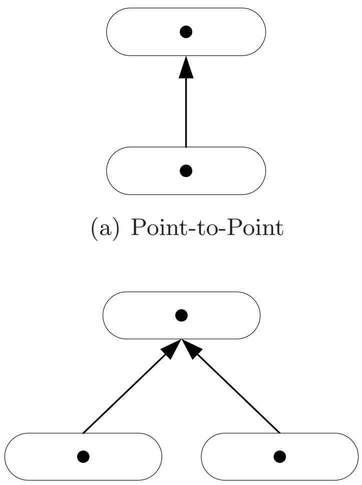

(a) Point-to-Point (b) Broadcast

(c) Multiple access (d) Interference channel

Figure 1.3: Different channel configurations

- Point-to-Point. The point-to-point channel is formed by means of a direct link between source and destination. In this configuration, multi-access scheme is not required.
- Broadcast. One source communicates with multiple destinations. For example, a base station communicates with a couple of mobile stations with the same information to all of them or different information to each of them.
- Multiple access. Multiple source nodes communicate with a single destination. A typical example is that multiple users communicate with the same base station.

- Interference channel. This is the most general case where multiple source nodes transmit to multiple destinations. Every destination is interfered by all sources.

The actual access for the broadcast, multiple access and interference channels can be coordinated by conventional multiple access methods. These can be classified into reservation-based and contention-based schemes [9]. The former is mainly used in centralized systems where radio resources can be reserved a priori and where the traffic is regular. The latter is applied in decentralized systems, where all nodes need to compete for the radio resources before transmission. Reservation-based schemes include:

- Time division multiple access (TDMA). Different user and relay information streams are scheduled in time, where different link is assigned to different time slot. For example, the direct link from the source to destination transmit in the first time slot and relay transmits in second time slot.

- Frequency division multiple access (FDMA). Different user and relay information streams are scheduled in different frequency band. For example, the direct link from the source to destination is assigned to frequency channel one and relay link uses frequency channel two.

- Code division multiple access (CDMA). Different user and relay information streams are separated via orthogonal spreading codes. For example, the direct link from the source to destination is assigned one spreading code and relay link uses another spreading code. CDMA allows all streams transmit in the same frequency band at the same time, so accurate power control is need to prevent one stream overwhelming another one due to near-far problem. This is often hard to implement in context of cooperative communications [6].

- Orthogonal Frequency Division Multiple Access (OFDMA). Different user and relay information streams are assigned to different subcarriers or resource blocks. For example, one node may act as both a source and a relay, its own data and relayed data of a cooperative node are assigned to different subcarriers.

- Multicarrier CDMA (MC-CDMA). Different user and relay information streams use different orthogonal spreading codes across several subcarriers or over several data symbols at a fixed subcarrier.

In the case of contention-based schemes, all the sources and relays are assumed to use the same frequency band and code and compete for the resource in time. The main types of contention-based scheme are:

- Aloha. The earliest and the most simple contention-based scheme. The key idea is that whenever a node has something to send, it sends. When a packet is received by the central, an acknowledgment is sent back in broadcast. If the sending node does not receive an acknowledgment within a set time, a collision is assumed and it retransmits within a random time slot.

- Carrier sense multiple access (CSMA). also known as “listen before talk”. A node verifies the availability of the channel. If the channel is free, it starts to send. If the channel is busy the node waits for the transmission in progress to finish before initiating its own transmission.

1.4 Previous related work

Foundational work on multiple-access interference channels was published in [7], [10], where correlated fading and interference are found to significantly degrade the performance in simulated channels. Blum published a journal article on MIMO capacity under interference [11], which includes the mutual information expressions of interference-impaired MIMO channels and the optimum power allocation strategy among transmit antennas under different signal to interference power ratio. In [12], the author introduced that when the array response vector (i.e. the spatial signature) of the desired signal is nearly co-linear with the array response vector of interference, the signal to interference and noise ratio will be degraded. In [13], authors used an experimental approach to measure the throughput of an MIMO system under interference. Various levels of spatial correlation between the intended signal and interference are tested by manually separating the transmitters and receivers. However, very little work has been carried out to model this correlation. Recently, Czink et al. [8] present an analytical multiuser MIMO channel model that is able to model interference in the spatial domain. The proposed model characterizes the amount of eigenspace alignment on a continuous scale between fully aligned and maximally non-aligned by smoothly rotating the eigenspace of the interference correlation matrix.

To better utilize the resources in spatial domain, spatial scheduling techniques are used to leverage substantial gains in spectral efficiency and system throughput. An algorithm to find the group of users for SDMA mode based on the wideband average spatial correlation is proposed in [14]. [15] and [16] proposed determinant pairing scheduling and orthogonal pairing scheduling schemes, that aim to maximize MIMO capacity and find the two users of best orthogonality respectively.

1.5 Contributions and organization

My work is based on the multi-user MIMO channel model in [8] making extensive use of the mutual information metric. In Chapter 2, the channel model is reviewed and new evaluations of mutual information increase and multi-user interference are considered. I parameterized the multi-user MIMO channel model from radio channel measurements, including both indoor-to-indoor and indoor-to-outdoor scenarios in Chapter 3. In Chapter 4, I designed a user grouping scheme for uplink multi-access channels. The scheme is consisting of a round robin scheduler and a grouping criteria building on the mutual information metric. The main contributions of this thesis can be summarized as follows:

- I quantified the mutual information increase using the mutual information metric. The relevance between the eigenvalue structures of the receiver correlation matrices and the increase of mutual information is evaluated and a explicit expression is given.

- I introduced a novel metric based on the geodesic distance between correlation matrices.

- I evaluated the case where a user is affected by multi-user interference and found how the subspace similarity of the multiple interferences influences the mutual information metric.

- I parameterized the multi-user MIMO channel model from radio channel measurements. For indoor-to-indoor scenarios, the distribution of the mutual information metric is specific with respect to the movement of the receiver. For indoor-to-outdoor scenarios, the correlation matrices of different users in the same building are found to be similar.

- I proposed an uplink user grouping scheme using the mutual information metric. This scheme is able to offer gains in spectral efficiency and system throughput. I compared the performance of the proposed scheme with other schemes. Simulation results show that this scheme outperforms other schemes in some cases.

CHAPTER 2

Multi-User MIMO Channel modeling

The analytical channel model [8], [17] is reviewed in this chapter, including the metrics of eigenspaces compatibility between desired and undesired channel matrices, and an analytical way to model the smooth transition of the eigenspaces of the interference channel.

2.1 MIMO mutual information with interference

First, to quantify the effect of different subspace alignment in order to be able to model it accordingly, an interference-impaired MIMO link is modeled by

$$\mathbf{y} = \mathbf{H}_0\mathbf{x}_0 + \sum_{i=1}^{N} \mathbf{H}_i\mathbf{x}_i + \mathbf{n}, \tag{2.1}$$

where $\mathbf{H}_0$ denotes the channel matrix of the intended channel, $\mathbf{H}_i$ denotes the N interfering channels, $i \in \{1, \ldots, N\}$, and $\mathbf{n} \sim \mathcal{CN}(0, \sigma_N^2\mathbf{I})$ is complex symmetric white Gaussian noise. We assume that the transmitted symbols are uncorrelated and have unit variance, i.e., $\mathrm{E}\left\{\mathbf{x}_\mathrm{i}\mathbf{x}_\mathrm{i}^\mathrm{H}\right\} = \mathbf{I}$, $i \in \{1, \ldots, N\}$.

Furthermore, we assuming that Gaussian signaling at all transmitters, perfect channel state information at the receivers and single-user detection (treating the interference as noise), the relevant expected mutual information between input $\mathbf{x}_0$ and output $\mathbf{y}$ of the interference-impaired channel in (2.1) is given by [11]

$$I = \mathrm{E}\left\{\log_2 \det\left(\mathbf{I} + \mathbf{H}_0\mathbf{H}_0^\mathrm{H}\left(\sum_{i=1}^{N} \mathbf{H}_i\mathbf{H}_i^\mathrm{H} + \sigma^2\mathbf{I}\right)^{-1}\right)\right\}. \tag{2.2}$$

2.2 Metrics

This section presents a set of metrics which are able to reflect the severity of spatial interference, including the interference-impaired mutual information metric[17], the Correlation Matrix Distance (CMD) [18] and the geodesic distance between correlation matrices. These metrics can be expressed by means of the channel receiver correlation matrices and achieve the maximum and minimum in certain extreme cases of correlation matrix eigenspace alignment.

2.2.1 Mutual information metric

This section reviews the mutual information metric proposed in [17]. The $D \times D$ correlation matrices at the receiver can be written as

$$\begin{aligned} \mathbf{R}_0 &= \mathrm{E}\left\{\mathbf{H}_0\mathbf{H}_0^{\mathrm{H}}\right\}, & (2.3)\\ \mathbf{R}_{\mathrm{I}} &= \mathrm{E}\left\{\sum_{i=1}^{N}\mathbf{H}_i\mathbf{H}_i^{\mathrm{H}}\right\}. & (2.4)\end{aligned}$$

Furthermore, $\mathbf{R}_0$ and $\mathbf{R}_{\mathrm{I}}$ can be written by their eigendecomposition

$$\begin{aligned} \mathbf{R}_0 &= \mathbf{U}\mathbf{\Lambda}\mathbf{U}^{\mathrm{H}}, & (2.5)\\ \mathbf{R}_{\mathrm{I}} &= \mathbf{V}\mathbf{\Gamma}\mathbf{V}^{\mathrm{H}}, & (2.6)\end{aligned}$$

where $\mathbf{U}$ and $\mathbf{V}$ are unitary matrices, and $\mathbf{\Lambda} = \mathrm{diag}(\lambda_1, \cdots, \lambda_{\mathrm{D}})$, $\mathbf{\Gamma} = \mathrm{diag}(\gamma_1, \cdots, \gamma_{\mathrm{D}})$, with sorted eigenvalues $\lambda_1 \geq \lambda_2 \geq \cdots \geq 0$ and $\gamma_1 \geq \gamma_2 \geq \cdots \geq 0$.

Similarly to (2.2), by substituting the Gram matrix with their expectation $\mathbf{R}_0$ and $\mathbf{R}_{\mathrm{I}}$, the mutual information metric is defined as

$$\begin{aligned} J(\mathbf{R}_0, \mathbf{R}_{\mathrm{I}}, \sigma^2) &= \log_2\det(\mathbf{I} + \mathbf{R}_0(\mathbf{R}_{\mathrm{I}} + \sigma^2\mathbf{I})^{-1}), & (2.7)\\ &= \log_2\det\left(\mathbf{I} + \mathbf{\Lambda}\mathbf{U}^{\mathrm{H}}\mathbf{V}\left(\mathbf{\Gamma} + \sigma^2\mathbf{I}\right)^{-1}\right)\mathbf{V}^{\mathrm{H}}\mathbf{U}\big) & (2.8)\\ &= \log_2\det\left(\mathbf{I} + \mathbf{\Lambda}\mathbf{T}\left(\mathbf{\Gamma} + \sigma^2\mathbf{I}\right)^{-1}\right)\mathbf{T}^{\mathrm{H}}\big), & (2.9)\end{aligned}$$

where $\mathbf{T} = \mathbf{U}^{\mathrm{H}}\mathbf{V}$ can be considered as a unitary coordinate transformation. In the following, σ is occasionally neglected for simplicity.

When $\mathbf{\Lambda}$ and $\mathbf{\Gamma}$ are given, The value of $J\left(\mathbf{R}_0, \mathbf{R}_{\mathrm{I}}\right)$ depends on the degree of alignment between the subspaces $\mathbf{U}$ and $\mathbf{V}$, which is quantified by the following theorem [8].

Theorem 1 *For all* $\mathbf{R}_0 = \mathbf{U}\mathbf{\Lambda}\mathbf{U}^{\mathrm{H}}, \mathbf{R}_{\mathrm{I}} = \mathbf{V}\mathbf{\Gamma}\mathbf{V}^{\mathrm{H}}$, *when* $\mathbf{R}_0$ *and* $\mathbf{\Gamma}$ *are fixed,* J *satisfies*

$$\underbrace{J(\mathbf{R}_0, \mathbf{U}\mathbf{\Gamma}\mathbf{U}^{\mathrm{H}})}_{J_{\min}(\mathbf{R}_0,\mathbf{\Gamma})} \leq J(\mathbf{R}_0, \mathbf{V}\mathbf{\Gamma}\mathbf{V}^{\mathrm{H}}) \leq J\underbrace{\left(\mathbf{R}_0, \overleftarrow{\mathbf{U}}\mathbf{\Gamma}\overleftarrow{\mathbf{U}}^{\mathrm{H}}\right)}_{J_{\max}(\mathbf{R}_0,\mathbf{\Gamma})} \tag{2.10}$$

for all unitary matrices $\mathbf{V}$.

$\overleftarrow{\mathbf{U}}$ is the column-wise reversed version of $\mathbf{U}$. The two extreme cases are achieved by $\mathbf{V} = \mathbf{U}$ (i.e., $\mathbf{T} = \mathbf{I}$) and $\mathbf{V} = \overleftarrow{\mathbf{U}}$ (i.e., $\mathbf{T} = \overleftarrow{\mathbf{I}}$). The minimum and maximum value are explicitly given by

$$J_{\min}(\mathbf{R}_0, \mathbf{\Gamma}) = \sum_{d=1}^{D} \log_2 \left(1 + \lambda_d(\sigma^2 + \gamma_d)^{-1}\right), \tag{2.11}$$

$$J_{\max}(\mathbf{R}_0, \mathbf{\Gamma}) = \sum_{d=1}^{D} \log_2 \left(1 + \lambda_{D+1-d}(\sigma^2 + \gamma_d)^{-1}\right). \tag{2.12}$$

Intuitively, when the eigenspaces of signal and interference are identical, the worst case occurs and thus, the strongest eigenmode of the intended signal is affected by the strongest eigenmode of interference. By contrast, the best case, corresponding to the largest mutual information metric, is achieved when the strongest eigenmode of the intended signal aligns with the weakest eigenmode of interference.

Furthermore, for the 2-dimensional case ($D = 2$), the correlation matrix $\mathbf{R}$ can be interpreted as an ellipse. The eigenvalues determine the length of the axes of the ellipse i.e., a larger condition number gives a narrow ellipse and when two eigenvalues are equal, the ellipse becomes a circle. The eigenvectors determine the rotation of the ellipse in space. Based on this interpretation, the worst case can be considered as the case that two ellipses fully overlap. Accordingly, the best case is obtained when two ellipse are narrow and orthogonal.

To focus on the role of the subspace compatibility, [8] further defines the scaled mutual information metric

$$\tilde{J}(\mathbf{R}_0, \mathbf{R}_\mathrm{I}) = \frac{J(\mathbf{R}_0, \mathbf{R}_\mathrm{I}) - J_{\min}(\mathbf{R}_0, \mathbf{\Gamma})}{J_{\max}(\mathbf{R}_0, \mathbf{\Gamma}) - J_{\min}(\mathbf{R}_0, \mathbf{\Gamma})}. \tag{2.13}$$

This measure is well-defined unless $J_{\min} = J_{\max}$, which occurs if for both channels all $\lambda_i = \lambda$. According to theorem 1, $\tilde{J}$ is bounded by

$$0 \leq \tilde{J}(\mathbf{R}_0, \mathbf{\Gamma}) \leq 1. \tag{2.14}$$

Theorem 2 *The scaled mutual information metric $\tilde{J}$ is invariant to the exchange of its arguments $\mathbf{R}_0$ and $\mathbf{R}_\mathrm{I}$, i.e.,*

$$\tilde{J}(\mathbf{R}_0, \mathbf{R}_\mathrm{I}) = \tilde{J}(\mathbf{R}_\mathrm{I}, \mathbf{R}_0). \tag{2.15}$$

This property allows us to think $\tilde{J}$ is a measure of subspace compatibility between signal and interference. I refer the interesting readers to [17] for more details regarding the proof of the two theorems.

2.2.2 Correlation matrix distance

The CMD was introduced in [17], [18] for the purpose of quantifying the distance between measured channel correlation matrices. The CMD is defined as

$$d(\mathbf{R}_0, \mathbf{R}_\mathrm{I}) = 1 - \frac{\mathrm{tr}\left\{\mathbf{R}_0, \mathbf{R}_\mathrm{I}\right\}}{\|\mathbf{R}_0\|_\mathrm{F} \cdot \|\mathbf{R}_\mathrm{I}\|_\mathrm{F}}. \tag{2.16}$$

The second term of this metric is the normalized inner product of two matrices. When $\mathbf{R}_0$ and $\mathbf{R}_\mathrm{I}$ are collinear, the metric gets the minimum value of 0. By contrast, the metric is maximized to 1 if $\mathbf{R}_0$ and $\mathbf{R}_\mathrm{I}$ are orthogonal to each other. Using the eigenvalue decompositions, it can be rewritten as

$$\begin{aligned} d(\mathbf{R}_0, \mathbf{R}_\mathrm{I}) &= 1 - \frac{\mathrm{tr}\left(\mathbf{\Lambda}\mathbf{U}^\mathrm{H}\mathbf{V}\mathbf{\Gamma}\mathbf{V}^\mathrm{H}\mathbf{U}\right)}{\sqrt{\mathrm{tr}\left(\Lambda^2\right)\mathrm{tr}\left(\Gamma^2\right)}} &(2.17)\\ &= 1 - \frac{\mathrm{tr}\left(\mathbf{\Lambda}\mathbf{T}\mathbf{\Gamma}\mathbf{T}^\mathrm{H}\right)}{\sqrt{\mathrm{tr}\left(\mathbf{\Lambda}^2\right)\mathrm{tr}\left(\mathbf{\Gamma}^2\right)}}, &(2.18)\end{aligned}$$

the bounds of the metric are given as follows.

Theorem 3 *For all* $\mathbf{R}_0 = \mathbf{U}\mathbf{\Lambda}\mathbf{U}^\mathrm{H}, \mathbf{R}_\mathrm{I} = \mathbf{V}\mathbf{\Gamma}\mathbf{V}^\mathrm{H}$*, when* $\mathbf{R}_0$ *and* $\mathbf{\Gamma}$ *are fixed,* d *satisfies*

$$\underbrace{d(\mathbf{R}_0, \mathbf{U}\mathbf{\Gamma}\mathbf{U}^\mathrm{H})}_{d_{\min}(\mathbf{R}_0,\mathbf{\Gamma})} \leq d(\mathbf{R}_0, \mathbf{V}\mathbf{\Gamma}\mathbf{V}^\mathrm{H}) \leq d\underbrace{\left(\mathbf{R}_0, \overleftarrow{\mathbf{U}}\mathbf{\Gamma}\overleftarrow{\mathbf{U}}^\mathrm{H}\right)}_{d_{\max}(\mathbf{R}_0,\mathbf{\Gamma})} \tag{2.19}$$

for all unitary matrices $\mathbf{V}$*.*

The two extreme cases are realized by $\mathbf{V} = \mathbf{U}$ (i.e., $\mathbf{T} = \mathbf{I}$) and $\mathbf{V} = \overleftarrow{\mathbf{U}}$ (i.e., $\mathbf{T} = \overleftarrow{\mathbf{I}}$). See [8] for proof.

2.2.3 Geodesic distance between correlation matrices

Additionally to the previous work, this thesis introduces another metric: the geodesic distance between correlation matrices[1]. One of the advantages of this metric is the fact that it exploits the geometry of the domain space, which is the set of Hermitian positive definite matrices. This section presents the basic differential geometry concepts that are used. As shown in [19], the set of Hermitian positive definite matrices $\mathcal{S} = \left\{\mathbf{R} \in \mathcal{C}^{n\times n} : \mathbf{R} = \mathbf{R}^\mathrm{H}, \mathbf{R} \succ 0\right\}$ is a convex cone.

The geodesic curve $P(t)$, which is the shortest path connecting two points $\mathbf{R}_1$ and $\mathbf{R}_2$ in the set $\mathcal{S}$ with all its points belonging to $\mathcal{S}$, is given by [19], [20]

$$P(t) = \mathbf{R}_1^{1/2}\exp(t\mathbf{C})\mathbf{R}_1^{1/2}, \tag{2.20}$$

[1] In the following we assume that the channel correlation matrix is strictly positive definite.

where $\mathbf{C} = \mathbf{C}^{\mathrm{H}} = \log(\mathbf{R}_1^{-1/2}\mathbf{R}_2\mathbf{R}_1^{-1/2})$, hence, $P(0) = \mathbf{R}_1$, $P(1) = \mathbf{R}_2$. The derivative of the geodesic at $t = 0$, which is actually the direction of the curve at $t = 0$, is given by the Hermitian matrix $\dot{P}(0) = \mathbf{R}_1^{1/2}\mathbf{C}\mathbf{R}_1^{1/2}$, called speed matrix.

The geodesic distance between any two points in $\mathcal{S}$ is defined as the the length of the geodesic curve connecting them. It is given by [19], [20]

$$D_{\mathrm{g}}(\mathbf{R}_1, \mathbf{R}_2) = \|\mathbf{C}\|_{\mathrm{F}} \,, \tag{2.21}$$

equivalently, it also can be rewritten as

$$D_{\mathrm{g}}(\mathbf{R}_1, \mathbf{R}_2) = \left(\sum_i |\log\eta_i|^2\right)^{1/2} , \tag{2.22}$$

where η_i are the eigenvalues of matrix $\mathbf{R}_1^{-1/2}\mathbf{R}_2\mathbf{R}_1^{-1/2}$.

Based on the verification by simulations, we conjecture that $\mathbf{R}_0 = \mathbf{U}\mathbf{\Lambda}\mathbf{U}^{\mathrm{H}}, \mathbf{R}_{\mathrm{I}} = \mathbf{V}\mathbf{\Gamma}\mathbf{V}^{\mathrm{H}}$, when $\mathbf{R}_0$ and $\mathbf{\Gamma}$ are fixed, D_{g} satisfies

$$\underbrace{D_{\mathrm{g}}(\mathbf{R}_0, \mathbf{U}\mathbf{\Gamma}\mathbf{U}^{\mathrm{H}})}_{D_{\mathrm{gmin}}(\mathbf{R}_0,\mathbf{\Gamma})} \leq D_{\mathrm{g}}(\mathbf{R}_0, \mathbf{V}\mathbf{\Gamma}\mathbf{V}^{\mathrm{H}}) \leq D_{\mathrm{g}}\underbrace{(\mathbf{R}_0, \overleftarrow{\mathbf{U}}\mathbf{\Gamma}\overleftarrow{\mathbf{U}}^{\mathrm{H}})}_{D_{\mathrm{gmax}}(\mathbf{R}_0,\mathbf{\Gamma})} \tag{2.23}$$

for all unitary matrices $\mathbf{V}$. However, no close form proof has been found yet.

D_{g} can be normalized to the range of $[0, 1]$ as previously done

$$\tilde{D_{\mathrm{g}}}(\mathbf{R}_0, \mathbf{R}_{\mathrm{I}}) = \frac{D_{\mathrm{g}}(\mathbf{R}_0, \mathbf{R}_{\mathrm{I}}) - D_{\mathrm{gmin}}(\mathbf{R}_0, \mathbf{\Gamma})}{D_{\mathrm{gmax}}(\mathbf{R}_0, \mathbf{\Gamma}) - D_{\mathrm{gmin}}(\mathbf{R}_0, \mathbf{\Gamma})}. \tag{2.24}$$

The two extreme cases are realized by $\mathbf{V} = \mathbf{U}$ (i.e., $\mathbf{T} = \mathbf{I}$) and $\mathbf{V} = \overleftarrow{\mathbf{U}}$ (i.e., $\mathbf{T} = \overleftarrow{\mathbf{I}}$).

The feature of this metric is the fact that it directly measures the distance between two correlation matrices in curved space, which is the set of Hermitian positive definite matrices.

2.2.4 Other Metrics

All the previous metrics are able to provide a measure of spatial compatibility in interference-impaired MIMO communication. Besides these metrics, the model also works well with other alternative metrics that fulfill the following requirements [8]:

- The metric depends on $\mathbf{R}_0 = \mathbf{U}\mathbf{\Lambda}\mathbf{U}^{\mathrm{H}}$, $\mathbf{R}_{\mathrm{I}} = \mathbf{V}\mathbf{\Gamma}\mathbf{V}^{\mathrm{H}}$.
- For fixed $\mathbf{R}_0 = \mathbf{U}\mathbf{\Lambda}\mathbf{U}^{\mathrm{H}}$, the extreme values are reached when $\mathbf{V} = \mathbf{U}$ and $\mathbf{V} = \overleftarrow{\mathbf{U}}$.
- The metric is continues with $\mathbf{V}$.

2.3 Modeling the multi-user channel subspaces

Upper and lower bounds of system performance are determined by the eigenvalue structure of $\mathbf{R}_0$ and $\mathbf{R}_\mathrm{I}$ as described in Theorem 1. As indicated, the performance is also strongly affected by the relative alignment of the their eigenspaces. In order to test MU MIMO algorithms for their performance, different MU channels may need to be tested under different level of signal subspace alignments for a certain interference severity.

Following [8], we focus on the channel described by (2.1) with receive correlation matrices $\mathbf{R}_0 = \mathbf{U}\mathbf{\Lambda}\mathbf{U}^\mathrm{H}$ and $\mathbf{R}_\mathrm{I} = \mathbf{V}\mathbf{\Lambda}\mathbf{V}^\mathrm{H}$, assuming that the receive correlation $\mathbf{R}_0$ of signal and the eigenvalue profile $\mathbf{\Gamma}$ are specified. These can be obtained from a measurement or a link model. Furthermore, a target value of metric giving the interference severity needs to be specified. Finally the model generates a suitable $\mathbf{V}$ such that the metric meets the target.

In the following, the procedure is explained in detail for the scaled mutual information metric $\tilde{J}$. It is applicable for every metric that satisfies the requirements introduced in Section 2.2.4.

2.3.1 Geodesic between unitary matrices

This section presents the basic differential geometry concepts that are used in modeling subspaces. Let us discuss the case that $\mathcal{U}(n)$ is a set of unitary matrices with size $n \times n$, which satisfies

$$\mathcal{U}(n) = \left\{ \mathbf{U} \in \mathcal{C}^{n\times n} : \mathbf{U}^\mathrm{H}\mathbf{U} = \mathbf{I}_n \right\} \tag{2.25}$$

The set of $\mathcal{U}(n)$ is a Lie group [21], which means $\mathcal{U}(n)$ has algebraic group structure, consisting of matrix multiplication operation m, inverse operator i and an identity element e, such that for every $\mathbf{U}_1, \mathbf{U}_2 \in \mathcal{U}(n)$, it holds [22]

1. $m(\mathbf{U}_1, \mathbf{U}_2) \in \mathcal{U}(n)$,
2. $m(\mathbf{U}_1, i(\mathbf{U}_2)) = m(i(\mathbf{U}_1), \mathbf{U}_2) = e$,
3. $m(\mathbf{U}_1, e) = m(e, \mathbf{U}_1) = \mathbf{U}_1$.

The Lie algebra $\mu(n)$ associated to unitary group is made of skew-Hermitian matrices, given by

$$\mu(n) = \left\{ \mathbf{u} \in \mathcal{C}^{n\times n} : \mathbf{u}^\mathrm{H} = -\mathbf{u} \right\} \tag{2.26}$$

The set $\mathcal{U}(n)$ also possesses a compatible differential manifold structure, which is considered to be a Riemannian manifold. The tangent space of the manifold at a point $\mathbf{U} \in \mathcal{U}(n)$ is denoted by $\mathrm{T}_\mathbf{U}\mathcal{U}(\mathrm{n})$. As a Riemannian manifold, $\mathcal{U}(n)$ is endowed with an inner product $\mathrm{Re}\{\mathrm{tr}(\mathbf{v_1}^\mathrm{H}\mathbf{v_2})\}$, associated to the Frobenius norm, for $\mathbf{v_1}, \mathbf{v_2} \in \mathrm{T}_\mathbf{U}\mathcal{U}(\mathrm{n})$.

Defining the length of a differentiable curve as [23]

$$l(C) = \int_0^1 \left\| \dot{C}(s) \right\|_{\mathrm{F}} \mathrm{d}s, \tag{2.27}$$

where $C \in \mathcal{U}(n)$ for $s \in [0,1]$, $\dot{C}(s)$ is the first derivative along the curve.

A geodesic between two unitary matrices $\mathbf{U}_1$ and $\mathbf{U}_2$ is a curve $\gamma(s)$ of minimal length such that $\gamma(0) = \mathbf{U}_1$, $\gamma(1) = \mathbf{U}_2$, i.e.,

$$l\left(\gamma_{\mathbf{U}_1 \to \mathbf{U}_2}\right) = \min_C l(C_{\mathbf{U}_1 \to \mathbf{U}_2}). \tag{2.28}$$

A geodesic curve emanating from the point $\mathbf{U}_1 \in \mathcal{U}(n)$ with tangent direction $\mathbf{v} \in \mathrm{T}_{\mathbf{U}}\mathcal{U}(\mathrm{n})$ has the expression $\gamma(s) = \mathbf{U}_1 \exp(s\mathbf{u})$ where $s \in [0,1]$, $\mathbf{u} = \mathbf{U}_1^{-1}\mathbf{v}$. Therefore, it holds $\dot{\gamma} = \gamma\mathbf{u}$, the geodesic path length is given by

$$D_\gamma = \int_0^1 \sqrt{\mathrm{tr}\left((\gamma(\mathrm{s})\mathbf{u})^{\mathrm{H}} \left(\gamma(\mathrm{s})\mathbf{u}\right)\right)}\mathrm{d}s \quad = \quad \|\mathbf{u}\|_{\mathrm{F}}\,. \tag{2.29}$$

If the geodesic curve $\gamma(s)$ is specified by two end points $\gamma(0) = \mathbf{U}_1$ and $\gamma(1) = \mathbf{U}_2$, the geodesic can be rewritten as [22]

$$\begin{aligned} \gamma(s) &= \mathbf{U}_1 \exp(s \log(\mathbf{U}_1^{\mathrm{H}})\mathbf{U}_2) \\ &= \mathbf{U}_1(\mathbf{U}_1^{\mathrm{H}}\mathbf{U}_2)^s \\ &= \mathbf{U}_1\mathbf{W}\mathrm{diag}(e^{js\varphi_1}, \ldots, e^{js\varphi_n})\mathbf{W}^{\mathrm{H}}, \end{aligned} \tag{2.30}$$

where $\mathbf{W}$ and φ_i are from the eigenvalue decomposition

$$\mathbf{U}_1^H\mathbf{U}_2 = \mathbf{W}\mathrm{diag}(e^{j\varphi_1}, \ldots, e^{j\varphi_n})\mathbf{W}^H, \tag{2.31}$$

with $\varphi_i \ \epsilon \ (-\pi, \pi]$. The corresponding geodesic distance between these two points is given by

$$\begin{aligned} D_\gamma(\mathbf{U}_1, \mathbf{U}_2) &= l(P_{\mathbf{U}_1 \to \mathbf{U}_2}) \\ &= \|\log(\mathbf{U}_1^{\mathrm{H}}\mathbf{U}_2)\|_F \\ &= \left(\sum_{i=1}^n \varphi_i^2\right)^{1/2}. \end{aligned} \tag{2.32}$$

2.3.2 Generation of a deterministic V

When the receive correlation $\mathbf{R}_0$ of the signal and the eigenvalue profile $\mathbf{\Gamma}$ of the interference are specified, the eigenspace $\mathbf{V}$ of interference is the only factor to determine the severity of interference. The purpose of this subsection is to find a suitable $\mathbf{V}$, that satisfies $\tilde{J}(\mathbf{R}_0, \mathbf{V\Gamma V}^{\mathrm{H}}) = \tilde{J}_{\mathrm{target}}$.

As shown in Section 2.2.1, $\tilde{J} = 1$ is achieved by $\mathbf{V} = \overleftarrow{\mathbf{U}}$, while $\tilde{J} = 0$ is attained by $\mathbf{V} = \mathbf{U}$. Thus, along the geodesic from $\mathbf{U}$ to $\overleftarrow{\mathbf{U}}$, there must exist a $\mathbf{V}$ that satisfies $\tilde{J}_{\mathrm{target}}$, if $0 < \tilde{J}_{\mathrm{target}} < 1$.

As given in (2.30), a geodesic connecting $\mathbf{U}_1$ and $\mathbf{U}_2$ is defined as

$$\begin{aligned}\gamma_{\mathbf{U}_1\to\mathbf{U}_2}(s) &= \mathbf{U}_1(\mathbf{U}_1^{\mathrm{H}}\mathbf{U}_2)^s \\ &= \mathbf{U}_1\mathbf{W}\mathrm{diag}(e^{js\varphi_1},\ldots,e^{js\varphi_n})\mathbf{W}^{\mathrm{H}},\end{aligned} \tag{2.33}$$

where $\gamma_{\mathbf{U}_1\to\mathbf{U}_2}(0)=\mathbf{U}_1$ and $\gamma_{\mathbf{U}_1\to\mathbf{U}_2}(1)=\mathbf{U}_2$.

For this specific case, let us define $\mathbf{U}_1=\mathbf{U}$ and $\mathbf{U}_2=\overleftarrow{\mathbf{U}}$, and the corresponding $\mathbf{V}$ along the geodesic is defined as

$$\mathbf{V}(s)=\gamma_{\mathbf{U}\to\overleftarrow{\mathbf{U}}}(s), \tag{2.34}$$

and the continuous function $\tilde{J}(s)$ is given by

$$\tilde{J}(s)=\tilde{J}(\mathbf{R}_0,\mathbf{V}(s)\mathbf{\Gamma}\mathbf{V}^{\mathrm{H}}(s)). \tag{2.35}$$

According to the above equation, there exists an $s^{'}\in[0,1]$ with $\tilde{J}(s^{'})=\tilde{J}_{\mathrm{target}}$. This $s^{'}$ can be found using the bisection method [24].

2.3.3 Generation of a random V

The previous method generates a deterministic $\mathbf{V}$ for a specific $\tilde{J}_{\mathrm{target}}$. However, there are infinitely many possible solutions. To be able to sample the entire solution space, the following approach can be used.

1. Generate a unitary matrix $\mathbf{Z}$ randomly.

2. Evaluate $\tilde{J}_{\mathbf{Z}}=\tilde{J}(\mathbf{R}_0,\mathbf{Z}\mathbf{\Gamma}\mathbf{Z}^{\mathrm{H}})$.

3. Select the geodesic

$$\mathbf{V}(s)=\begin{cases}\gamma_{\mathbf{U}\to\mathbf{Z}}(s) & \text{if} \quad \tilde{J}_{\mathrm{target}}\le\tilde{J}_{\mathbf{Z}}\\ \gamma_{\mathbf{Z}\to\overleftarrow{\mathbf{U}}}(s) & \text{if} \quad \tilde{J}_{\mathbf{Z}}<\tilde{J}_{\mathrm{target}}\end{cases} \tag{2.36}$$

   and the corresponding continuous function $\tilde{J}$

$$\tilde{J}(s)=\tilde{J}(\mathbf{R}_0,\mathbf{V}(s)\mathbf{\Gamma}\mathbf{V}^{\mathrm{H}}(s)). \tag{2.37}$$

4. Find the $s^{'}\in[0,1]$ satisfying $\tilde{J}(s^{'})=\tilde{J}_{\mathrm{target}}$ using the bisection method.

Along the geodesic $\gamma(s)$ in step 3, the value of $\tilde{J}$ is not necessarily monotonous. However, since the function $\tilde{J}(s)$ is continuous, there alway exists an $s^{'}$ on the selected geodesic in step 3, which satisfies $\tilde{J}(s^{'})=\tilde{J}_{\mathrm{target}}$.

2.4 Evaluation of the multi-user channel model

In this section, we first give an evaluation of the average mutual information of multi-user interference channels with different degree of alignment. The results show that the rotations of the eigenspaces have significant impact on the average mutual information. To capture this effect, the scaled mutual information metric $\tilde{J}$ is employed. In Section 2.4.2, the quality of this metric is evaluated by comparison with mutual information. After that, since a good consistency is found between the mutual information metric and the average mutual information, Section 2.4.3 evaluates the capacity increase in terms of $J_{\max} - J_{\min}$, with different influencing factors, i.e., structure of eigenvalues and SIR. With the knowledge of $J_{\max} - J_{\min}$, we can find out how large gain in capacity we can achieve by alignment of the eigenspaces of the channel matrices of the intended signal and of the interfering channel.

2.4.1 Average mutual information of multi-user interference channels

I adopt the same method as in [8] and [17], but simulating with $D = 2$ receive antennas, which is the most common antenna configuration in the rest of this thesis. As expected, the average mutual information changes strongly solely due to the rotations of the interference eigenspace. For low receive correlations, where the correlation matrix has a low condition number $\kappa = 1.8$, around 5% changes of mutual information are seen compared to the minimum value, while for high correlations with a large condition number $\kappa = 19$, changes of around 80% are possible.

It is also shown that the optimum signaling is sometimes different from the interference free cases. In particular, depending on the degree of alignment, a highly correlated channel will sometimes be desired and capacity will be achieved by putting all power into a single subchannel, rather than divide power equally among different subchannels.

2.4.2 Evaluation of the scaled mutual information metric $\tilde{J}$

The quality of the metric $\tilde{J}$ has been widely studied and verified in [8]. Using the same method but with $D = 2$ receive antennas, I evaluate the quality of the metric $\tilde{J}$ in (2.2.1) with respect to the expected mutual information I in (2.2) at $D = 2$. Since $\tilde{J}$ is limited in $[0, 1]$, [8] defines a scaled version of expected mutual information $\tilde{I}$ for comparison

$$\tilde{I}(\mathbf{R}_0, \mathbf{R}_\mathrm{I}) = \frac{I(\mathbf{R}_0, \mathbf{R}_\mathrm{I}) - I(\mathbf{R}_0, \mathbf{U}\boldsymbol{\Gamma}\mathbf{U}^\mathrm{H})}{I(\mathbf{R}_0, \overleftarrow{\mathbf{U}}\boldsymbol{\Gamma}\overleftarrow{\mathbf{U}}^\mathrm{H}) - I(\mathbf{R}_0, \mathbf{U}\boldsymbol{\Gamma}\mathbf{U}^\mathrm{H})}. \quad (2.38)$$

Similar to the results in [8], I found that the scaled approximation $\tilde{J}$ captures the behavior of the scaled mean mutual information $\tilde{I}$ very well.

In some special cases, the two even coincide.

2.4.3 Evaluation of capacity increase $J_{\max} - J_{\min}$

The alignment of the eigenmodes of the receive correlation matrices has significant impact on the capacity of the interference-impaired channel. In this section, we discuss the capacity increase $J_{\max} - J_{\min}$ by subspace alignment.

As interpreted in Section 2.2.1, the interference-impaired channel can be considered as two overlapping ellipses. The degree of alignment can be quantified by $\tilde{J}$, which is visualized as the angle of between two ellipses. the difference between two extreme cases is independent of the eigenspaces compatibility, which is only determined by the eigenvalue structure. According to (2.11) and (2.12), we can draw an explicit form of $J_{\max} - J_{\min}$, which is given by

$$J_{\max} - J_{\min} = \sum_{d=1}^{d=D} \log_2 \left(\frac{\sigma^2 + \gamma_d + \lambda_{D+1-d}}{\sigma^2 + \gamma_d + \lambda_d} \right) \tag{2.39}$$

This expression remains invariant when $\mathbf{R}_0$ and $\mathbf{R}_\mathrm{I}$ (i.e., γ_d and λ_d) are exchanged.

Fig. 2.1 gives the theoretical relationship between $J_{\max} - J_{\min}$ and the condition numbers according to (2.39) for the case with $D = 2$ antennas. The power of the intended signal and interferences are normalized to one. Both condition numbers are in the range of [1,100].

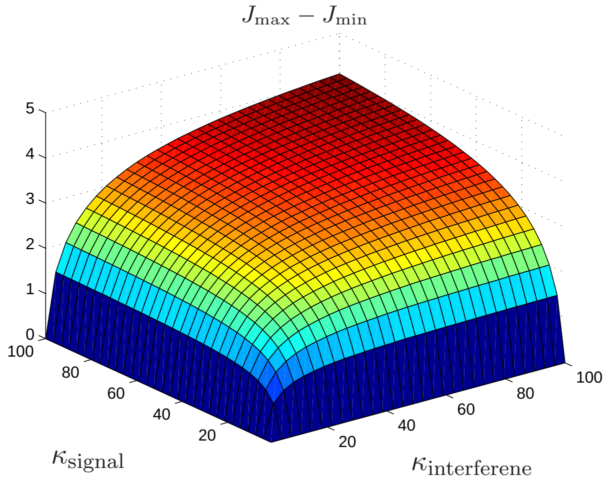

Figure 2.1: Relationship between $J_{\max} - J_{\min}$ and the condition numbers

It can be seen that the value of $J_{\max} - J_{\min}$ increases with both condition numbers. It becomes flat from the edges to the center, meaning that *the smaller condition number has greater impact on the value.* If we change the power ratio between the intended signal and interference, the figure is not symmetric to the diagonal anymore. Fig. 2.2 is obtained by setting different power to signal and interference. It is observed that the value of $J_{\max} - J_{\min}$ depends more on the one with larger power.

In conclusion, channels with large condition number are desired from interference alignment point of view. An interference-impaired channel with large $J_{\max} - J_{\min}$ and small $\tilde{J}$ is considered to be with larger potential capacity by taking the advantage of interference alignment.

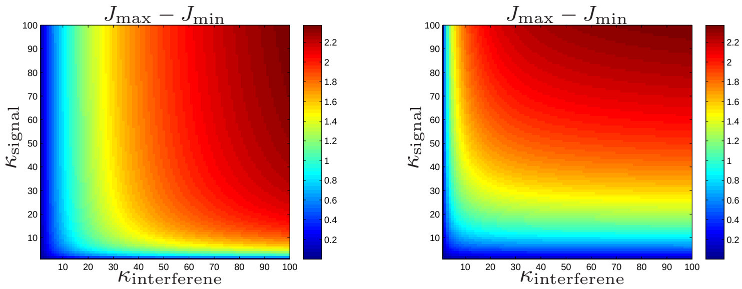

(a) Signal power is 10 times smaller than interference power

(b) Signal power is 10 times larger than interference power

Figure 2.2: Relationship between $J_{\max} - J_{\min}$ and the condition numbers

2.5 Modeling interference for multiple users

In wireless MIMO systems, one channel is often affected by more than one interfering channel. The most general case in the context of cooperative communications is that multiple source nodes transmit to multiple destinations. Each destination is affected by all other sources. In this section, the interference for multiple users will be studied. We found that the subspace similarity of the multiple interferences has great impact on channel capacity.

As a numerical example, let us consider the case where one intended channel is affected by two interferences with $D = 2$ antennas. Based on the eigendecomposition, the receiver correlation matrix of the intended channel can be written as

$$\mathbf{R}_0 = \mathbf{U}\boldsymbol{\Lambda}\mathbf{U}^{\mathrm{H}} \tag{2.40}$$

where $\mathbf{U}$ is uniformly chosen from unitary group and the diagonal elements of $\boldsymbol{\Lambda}$ are drawn from exponential distributions with mean $100\sigma^2$.

The receive correlation matrices of combined interference is given by

$$\begin{aligned} \mathbf{R}_{\mathrm{I}} &= \mathbf{R}_1 + \mathbf{R}_2 \quad &(2.41) \\ &= \mathbf{V}_1\boldsymbol{\Gamma}_1\mathbf{V}_1^{\mathrm{H}} + \mathbf{V}_2\boldsymbol{\Gamma}_2\mathbf{V}_2^{\mathrm{H}} \quad &(2.42) \end{aligned}$$

where $\mathbf{\Gamma_1}$ and $\mathbf{\Gamma_2}$ are drawn from exponential distributions with mean $50\sigma^2$. To demonstrate the impact of the orthogonality of interferences on the capacity of interference-impaired channel, two typical cases are considered. One is that two interferences are orthogonally addressed, i.e., $\mathbf{V}_1 = \overleftarrow{\mathbf{V}_2}$. In the other case, two interfering channels are colinear, where $\mathbf{V}_1 = \mathbf{V}_2$. Using the eigenvalue decompositions, $\mathbf{R}_\mathrm{I}$ can be written as $\mathbf{R}_\mathrm{I} = \mathbf{V\Gamma V}^\mathrm{H}$. We regenerate $\mathbf{V}$ as described in Section 2.3.2, varying s from 0 to 1, covering the worst and best case. At each

Fig. 2.3 plots the mutual information metric under different combined interferences by Monte-Carlo averaging of the modeled channels. For the combined interference consisting of two orthogonal interferences, the combining leads to a cancellation of two eigenvalue profiles, where the strongest eigenmode of $\mathbf{R_1}$ is averaged by the weakest eigenmode of $\mathbf{R_2}$ and vice versa. Therefore, the increase of mutual information using subspace alignment is not significant due to the two balanced eigenvalues of the combined interference. On the other hand when two interferences are colinear, two eigenvalue profiles are averaged by each other, i.e., the stronger eigenmode is averaged by another stronger eigenmode. In this way, the combined interference is with a medium condition number. To increase the capacity of intended channel, the orthogonal interferences should be coordinated.

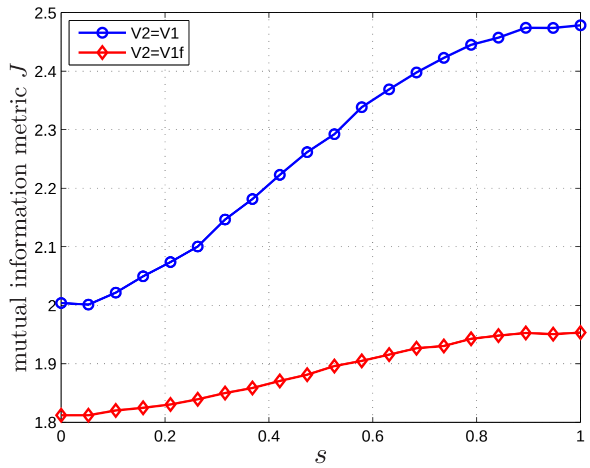

Figure 2.3: Mutual information metric under two different combinations of interferences

CHAPTER 3

Parameterization from measurements

Based on the previously introduced mutual information metric, we parameterize the multi-user MIMO model from radio channel measurements in this chapter. Two types of environments are investigated: peer-to-peer channels in an indoor office building, and indoor to outdoor multi-access channels.

3.1 Parameterization for indoor-to-indoor (I2I) scenarios

In this section, the model is parameterized from measurements in an I2I environment (see Appendix A.3). The distributions of the mutual information metric and the corresponding mutual information increase are given.

3.1.1 Distribution of scaled mutual information metric $\tilde{J}$

The first experimental parameterization is taken from the scenario where 4 nodes were moving locally over a small range and 4 nodes were static and each node is equipped with 2 antennas. The nodes were located as indicated in Fig. 3.1. Moving nodes are represented by circles and static nodes are denoted by squares. The scaled mutual information metric $\tilde{J}$ is calculated based on the receiver correlation matrices according to (2.2.1). The distributions of mutual information metric for different link pairs are shown in Fig. 3.2. There are four subplots each representing a specific receiver. We considered all pairs of links with a common receiver, denoted as $(m, n_1/n_2)$, where m is the index of the common receiver, n_1, n_2 is the index of two transmitters. We know that $\tilde{J}$ measures the degree of subspace alignment between signal and interference and it is invariant to the exchange

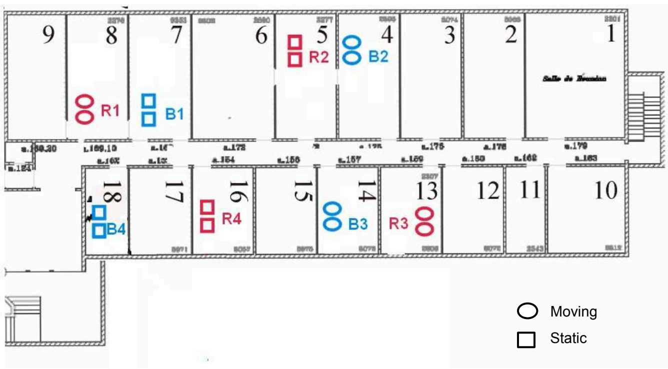

Figure 3.1: Map of 8 nodes I2I distributed scenarios

of two arguments (Theorem 2 in Section 2.2.1). For this reason, in the following, the link pair $(m, n_1/n_2)$ also equivalently represents the link pair $(m, n_2/n_1)$. In each subplot, all 6 different link pairs are investigated.

It can be observed that there are several distinct distributions. In the cases with a moving receiver, i.e. subset B2 and B3, it can be observed that the curves are flat and the distributions are nearly uniform, coving all the possible values from 0 to 1. This is for the reason that the channels become quite uncorrelated when the receiver moves from one position to another. The eigenspace and eigenvalue structure for both intended channel and interfering channel changed significantly during the course of movement. Correspondingly, $\tilde{J}$ varies rapidly. Fig. 3.3(a) shows a realization of $\tilde{J}$ and J associated with the corresponding upper bound $J_{\max}$ and lower bound $J_{\min}$ for the moving Rx case.

Furthermore, a moving Tx is also able to influence the angle of incident wave at Rx side, especially when the Tx is in close vicinity of the Rx, i.e., (B1, R1/R2). Fig. 3.3(b) shows the realizations of the $\tilde{J}$ and J with the upper bound $J_{\max}$ and lower bound $J_{\min}$ for the case when a moving Tx is close to a static Rx. In this case, $\tilde{J}$ performs similarly to the moving Rx case.

Fig. 3.3(c) shows the realizations for the case when a moving Tx is not in close vicinity to a static Rx, i.e., (B1, R2/R3). In this case, the fluctuation of $\tilde{J}$ caused by the movement is not significant. J keeps a stable relative position in between $J_{\max}$ and $J_{\min}$.

All static nodes leads to a very steep CDF, i.e., (B4, R2/R4). Fig. 3.3(d) shows the realizations for this case. We can observe that channels remained unchanged with time, which is expected for static channels.

In conclusion, for I2I scenarios, the distributions of $\tilde{J}$ (i.e., the degree of subspace alignment between signal and interference) can be classified by the steepness of them, which is determined by the movement of the nodes.

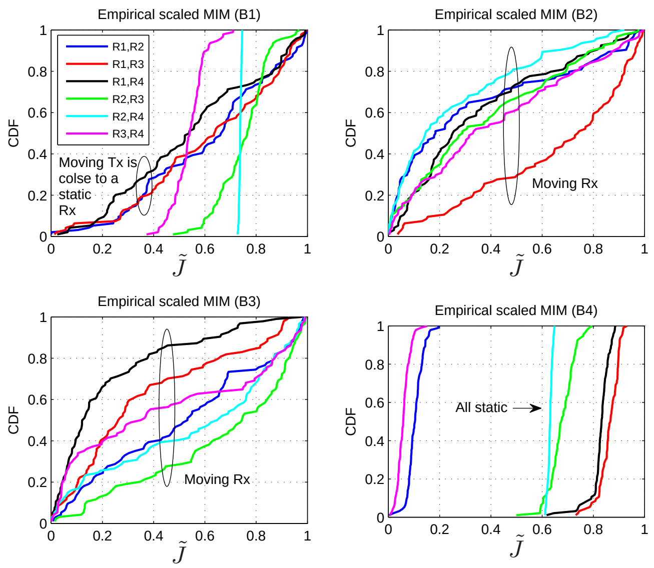

(a) Forward links where blue nodes as common receivers

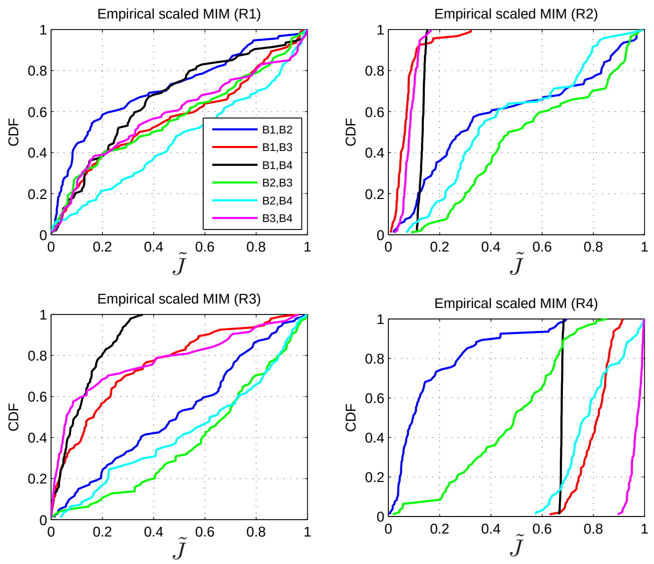

(b) Reverse links where red nodes as common receivers

Figure 3.2: Empirical distribution of scaled mutual information metric $\tilde{J}$

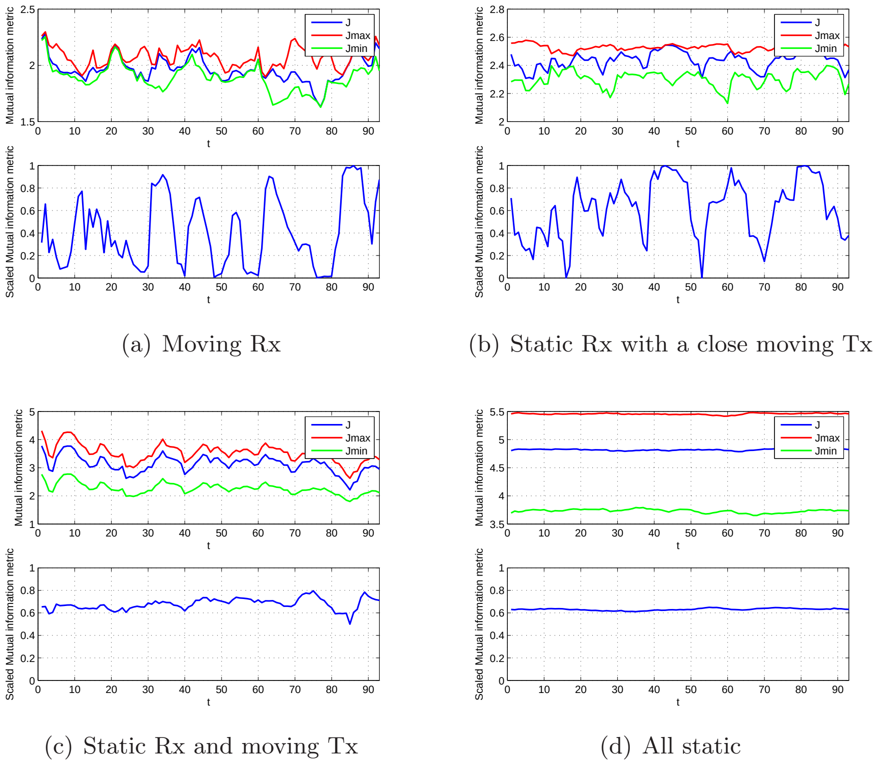

(a) Moving Rx

(b) Static Rx with a close moving Tx

(c) Static Rx and moving Tx

(d) All static

Figure 3.3: Realizations of J and $\tilde{J}$ in different cases of of I2I environment

3.1.2 Evaluation of $\tilde{J}$ and $J_{\max} - J_{\min}$

We have found that the beta distribution, defined on the interval $(0, 1)$ parameterized by two positive shape parameters a and b, is well matched with the empirical distribution of $\tilde{J}$,

$$
\begin{aligned}
p_\beta(\tilde{J}) &= \frac{1}{\mathrm{B(a, b)}} \tilde{J}^{(a-1)}(1-\tilde{J})^{(b-1)} && (3.1)\\
&= \frac{\Gamma(\mathrm{a}+\mathrm{b})}{\Gamma(\mathrm{a})+\Gamma(\mathrm{b})} \tilde{J}^{(a-1)}(1-\tilde{J})^{(b-1)} && (3.2)
\end{aligned}
$$

where $\mathrm{B}(\cdot)$ is the beta function, which equals to $\frac{\Gamma(\mathrm{a})}{\Gamma(\mathrm{a}+\mathrm{b})}$ and $\Gamma(\cdot)$ denotes the gamma function. The expected value μ of a Beta distribution random variable $\tilde{J}$ with parameters a and b are:

$$
\mu = \mathrm{E}(\tilde{J}) = \frac{a}{a+b} \tag{3.3}
$$

and variance $\mathrm{Var}(\tilde{J})$ is given by

$$
\mathrm{Var}(\tilde{J}) = \mathrm{E}(\tilde{J}-\mu)^2 = \frac{ab}{(a+b)^2(a+b+1)} \tag{3.4}
$$

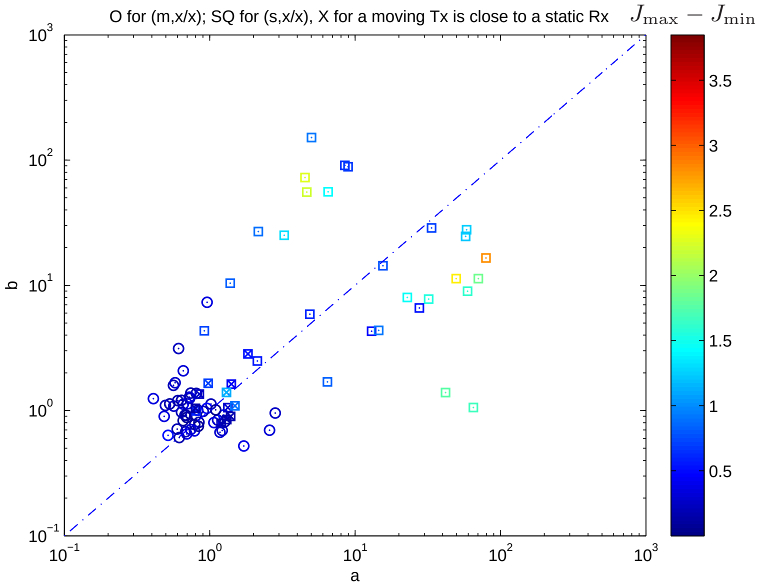

Figure 3.4: distribution of a and b

In Fig. 3.4, we use beta distribution to fit the metric statistics for all pairs of links shown in Fig. 3.2. Both two measurements for this scenario were investigated. The movement of the nodes are classified by the shape of the marker.

Circles and squares represent the cases with a moving Rx and a static Rx respectively. The markers with a 'x' inside are corresponding to the case where a moving Tx is close to a static Rx. It can be seen that circles and squares with 'x' are clustered with $a, b \sim 1$. In fact, according to the property of beta distribution, it becomes uniform distributed when $a = b = 1$. Obviously, this set of points is corresponding to the flat curves in Fig. 3.2. Moreover, most of these points are with a low $J_{\max} - J_{\min}$.

According to (3.3), we know that the points above the diagonal correspond to the pairs of links with mean of $\tilde{J}$ larger than 0.5. Below the diagonal, the points are related to the link pairs with a mean value smaller than 0.5.

Another scatter plot of $\mathrm{E}(\tilde{J})$ versus $\mathrm{Var}(\tilde{J})$ more intuitively shows the clusters of $\tilde{J}$ in Fig. 3.5. We investigated both two measurements for the same scenario to collect more data. According to (3.4), an upper bound for variance is given by

$$B_{\text{var}}(\mu) = \lim_{a,b \to 0} \mu(1-\mu)\frac{1}{a+b+1} = \mu(1-\mu) \tag{3.5}$$

All points below this bound are able to be well fitted by beta distribution. It can be observed that the flat curves in Fig. 3.2 are all clustered at the top

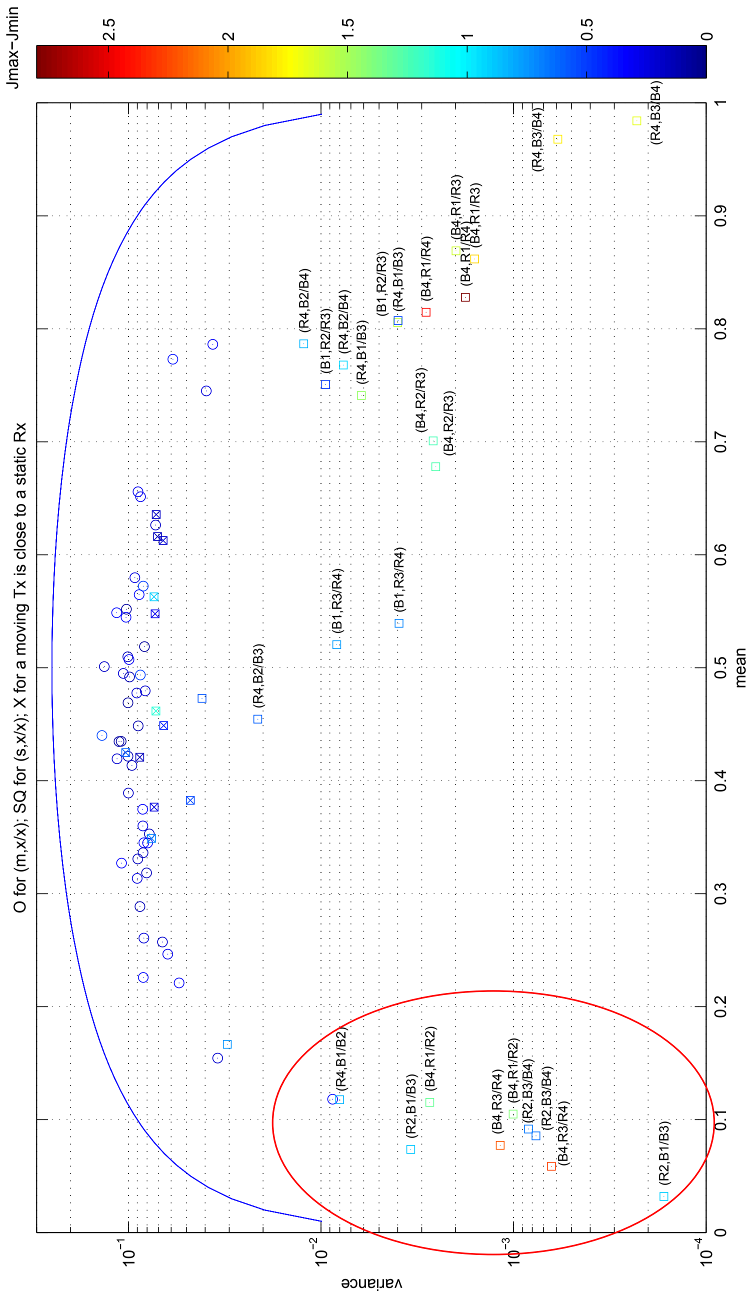

Figure 3.5: Mean versus variance of $\tilde{J}$

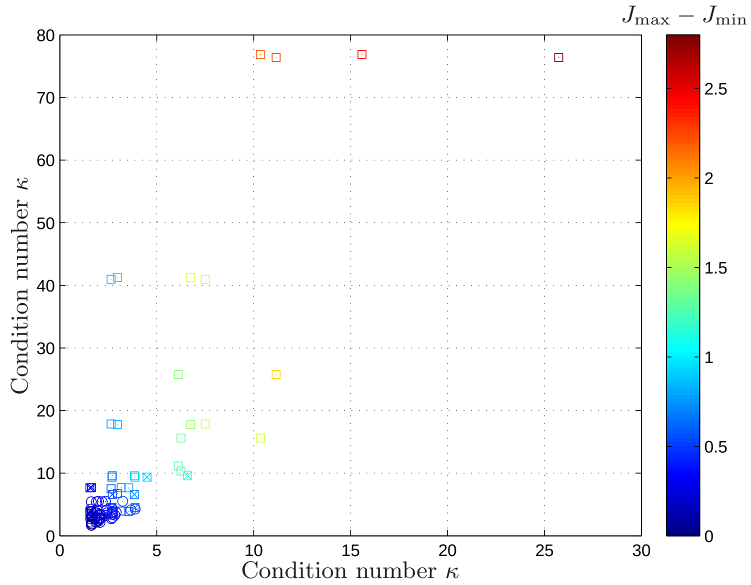

Figure 3.6: Rlation of condtional numbers and $J_{\max} - J_{\min}$

with a large variance. The points with either a large mean or a small mean are always associated with a relatively large $J_{\max} - J_{\min}$. The link pairs of interest are those points with a large $J_{\max} - J_{\min}$ and a small $\tilde{J}$, shown by the red ellipse. These pairs of links have large potential capacity and small amount of alignment between the two links. Thus, mutual information can be greatly improved by appropriate alignment of the eigenmodes of their correlation matrices.

Since different link pairs have different $J_{\max} - J_{\min}$ value. As discussed in Section 2.4.3, the mutual information increase $J_{\max} - J_{\min}$ is only determined by the eigenvalue structure of the receiver correlation matrices. In the following, we would like to analyze this relationship from real measurements.

Fig. 3.6 shows the relation of channel condition numbers versus $J_{\max} - J_{\min}$. The condition number is computed from correlation matrices, by averaging all condition numbers for a certain link over time. It can be seen that the color becomes warm with the increase of condition numbers, which matches well with the theory (c.f. Fig. 2.1). The contributions to the low condition number channels are mainly from moving Rx cases. The channels with large condition numbers (rank deficient) from highly correlated channels, which give large capacity increase $J_{\max} - J_{\min}$, are of interest. By appropriate alignment of the subspaces between these channels, we can gain capacity greatly, since less power will leakage to the unwanted subspace.

3.2 Parameterization for indoor-to-outdoor (I2O) scenarios

Measurements were taken in our indoor-to-outdoor environment as summarized in Appendix A.4. Eight nodes were moving locally over a small range in an office building, as shown in Fig. A.3, while a BS was on the last floor of another building. The distributions of the mutual information metric of different link pairs are shown in Fig. 3.7(a). All 8 links are investigated for this scenario. According to Theorem 2 in Section 2.2.1, we get 28 distinct link pairs. It can be seen that the distribution is centered at small means of $\tilde{J}$ and located close to each other. This means that their eigenspces of the receive correlation matrices are similar and all these links have strongly overlapped subspaces. A possible explanation for this effect would be that the incident angles for these links are similar from the BS viewpoint. The outdoor environment is lacking-scattering and thus the signals form different nodes reach the receiver through similar paths. As a result, the similarity between the receive correlation matrices is increased.

The results of large scale motion are shown in Fig. 3.7(b). The distribution of $\tilde{J}$ is similar to small scale motion case except that it spreads out a bit. Realizations for the two cases are depicted in Fig. 3.8.

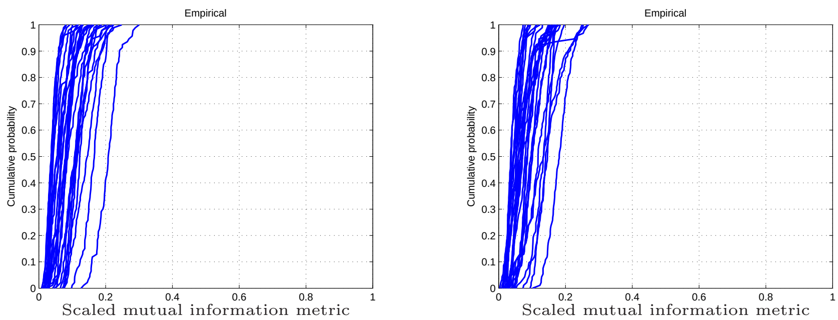

(a) Small scale motion

(b) Large scale motion

Figure 3.7: Empirical distribution of scaled mutual information metric $\tilde{J}$

The value of $J_{\max} - J_{\min}$ corresponding to each link pair is shown in Fig. 3.9. We found that the values are large as expected and thus considerable improvement can be made by appropriate alignment of the eigenmodes of correlation matrices.

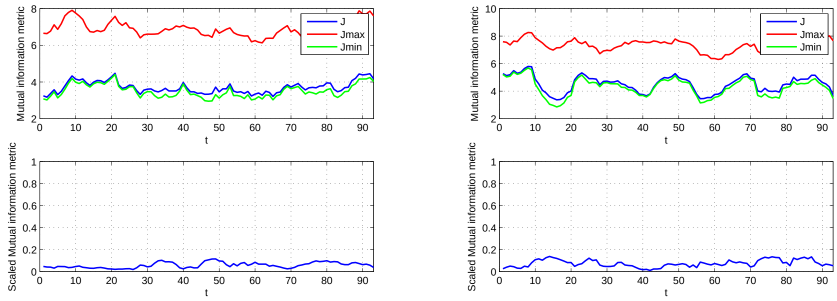

(a) Small scale motion (b) Large scale motion

Figure 3.8: Realizations of J and $\tilde{J}$ in different cases of I2O environment

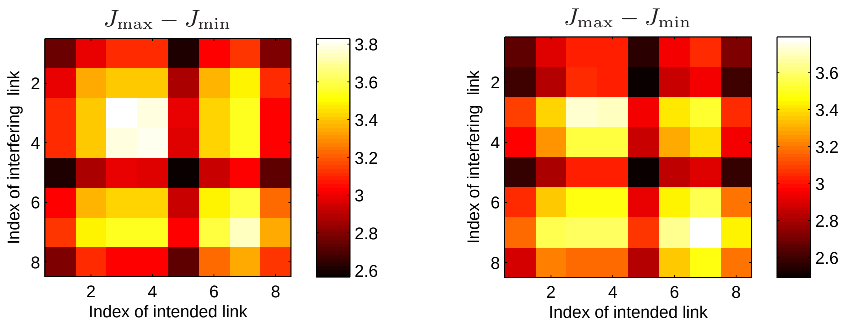

(a) Small scale motion (b) Large scale motion

Figure 3.9: $J_{\max} - J_{\min}$ for all link pairs in different cases

3.3 Parameterization at the existence of multiple interferences

The previous results were obtained considering that there exists only *one* interference. In the following, we will consider *multiple* interfering users and three typical cases are investigated. We use data of the static environment to analyze the behavior of the metric. The measurement is taken from the scenario where all 8 nodes were static with no people in the area and each node is equipped with 2 antennas.

3.3.1 Case study 1

Fig. 3.10 plots the CDF of scaled mutual information metric $\tilde{J}$ in the cases when two interfering channels affect the intended channel respectively and two interfering channels affect the intended channel simultaneously. The power of intended channel, two interfering channels and the combined interfering channel is normalized to one.

It can be observed from the distributions of $\tilde{J}$ that both of two interfering channels B1 and B4 are fairly orthogonal to the intended channel B3. In addition, the combined interference, denoted as B1&B4, is even more orthogonal to the signal. As discussed in Section 2.5, the subspace similarity of the multiple interferences is a crucial factor to determine channel capacity. The knowledge of the orthogonality between two interferences, in terms of $\tilde{J}$, will be of great importance. Therefore, in Fig. 3.11, the distribution of $\tilde{J}$ is depicted showing the orthogonality between B1 and B4.

Interestingly, although the subspaces of both two interferences are fairly orthogonal to signal subspaces, the subspaces of two interferences are *not similar* to each other. In the following, we link all above results in the receive signal space, illustrated in Fig. 3.14. 2×2 MIMO channels give 2 dimensional subspaces of the receive signal space.

In the receive signal space, signals of B1 and B4 are at opposite direction of the normal of intended signal B3. Adding up B1 and B4 causes a cancellation, which yields a more orthogonal combined interference with lower condition number. Tab. 3.13 lists the condition numbers before and after combining. A small condition number of B1&B4 indicates that both two eigenchannels of the intended signal are affected by the combined interference. Thus, the mutual information metric J decreases, as shown in Fig. 3.12, even though $\tilde{J}$ is increased.

3.3.2 Case study 2

Fig. 3.15 shows the CDF of scaled mutual information metric $\tilde{J}$ when two interfering channels affect the intended channel respectively and two interfering channels affect the intended channel simultaneously. Similarly to case 1, it can be observed from the distributions of $\tilde{J}$ that the two interfering channels B2 and B3, and the sum of B2 and B3, denoted as B2&B3 are all orthogonal to the intended channel B1. Moreover, the subspaces of two interferences are also similar to each other since $\tilde{J}$ between them, as shown in Fig. 3.16, is quite low. The corresponding receive signal space is illustrated in Fig. 3.19. It can be seen that signals of B2 and B3 are at the same direction to the normal of intended signal B1. Adding up B2 and B3 yields a a combined interference in between of them with a moderate condition number. Tab. 3.18 lists the condition numbers before and after combining. The combined interference stay the same, hence the mutual information metric J also remains unchanged, as shown in Fig. 3.17.

3.3.3 Case study 3

Fig. 3.20 shows the CDF of scaled mutual information metric $\tilde{J}$ of this case when two interfering channels affect the intended channel respectively and two interfering channels affect the intended channel simultaneously. We can observe that the signal from R1 is orthogonal to the intended signal R3, while the signal of R4 is collinear to R3. Adding up R1 and R4 will cause a strong cancellation, yielding a combined interference lying in between with a lower condition number. Fig. 3.22 depicted the corresponding receive signal space and the condition numbers are given in Tab. 3.1. The same as case 1, the combined interference goes to both eigenchannels of the intended link, so the mutual information metric J decreases, which is shown in Fig. 3.21.

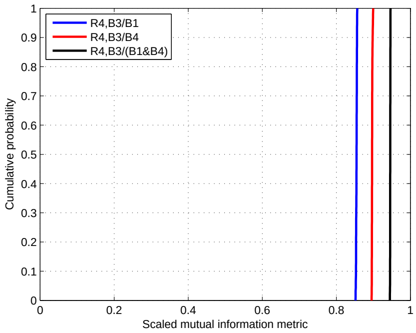

Figure 3.10: Case 1: Distributions of $\tilde{J}$ between signal and interferences

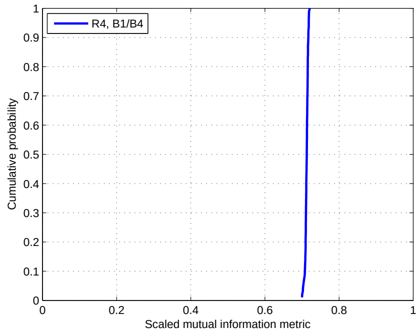

Figure 3.11: Case 1: Distributions of $\tilde{J}$ between two interferences

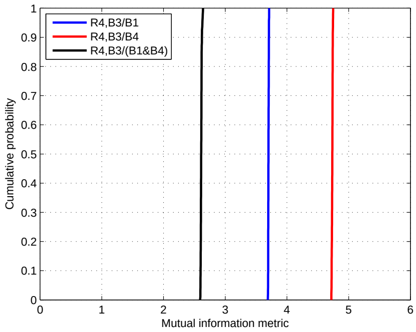

Figure 3.12: Case 1: Distributions of J between signal and interferences

Channel	Condition number
B1	15.9
B4	42.9
B1&B4	4.5

Figure 3.13: Case 1: Condition numbers

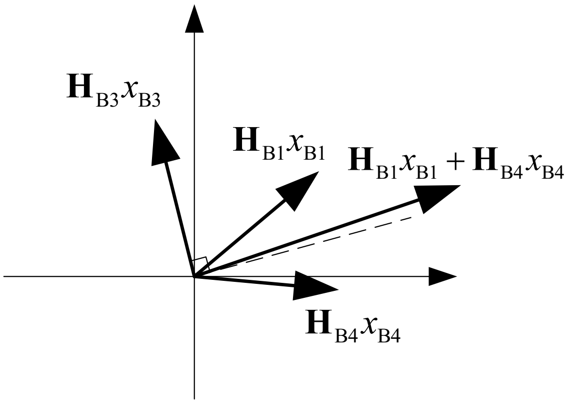

Figure 3.14: Case 1: Receive signal space

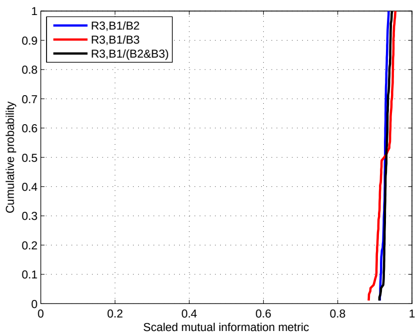

Figure 3.15: Case 2: Distributions of $\tilde{J}$ between signal and interferences

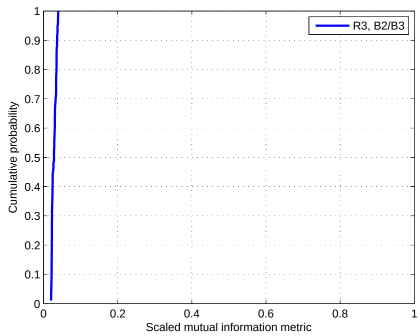

Figure 3.16: Case 2: Distributions of $\tilde{J}$ between two interferences

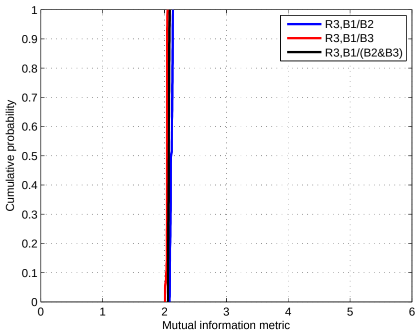

Figure 3.17: Case 2: Distributions of J between signal and interferences

Channel	Condition number
B2	2.1
B3	1.9
B2&B3	2

Figure 3.18: Case 2: Condition numbers

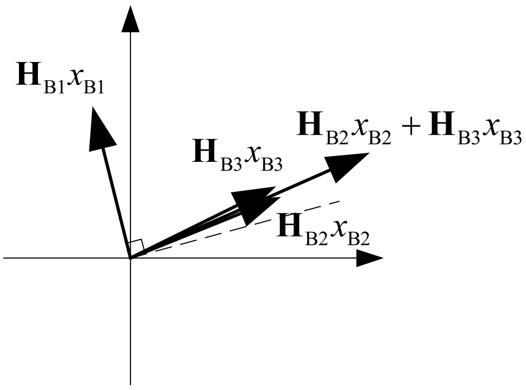

Figure 3.19: Case 2: Receive signal space

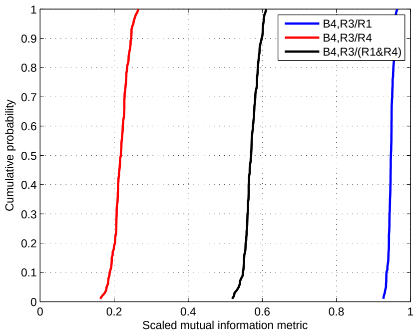

Figure 3.20: Case 3: Distributions of $\tilde{J}$ between signal and interferences

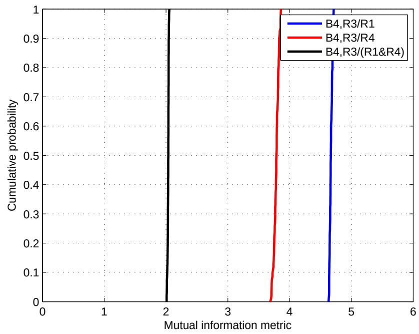

Figure 3.21: Case 3: Distributions of J between signal and interferences

Channel	Condition number
R1	35
R4	76.3
R1&R4	3.1

Table 3.1: Case 3: Condition numbers

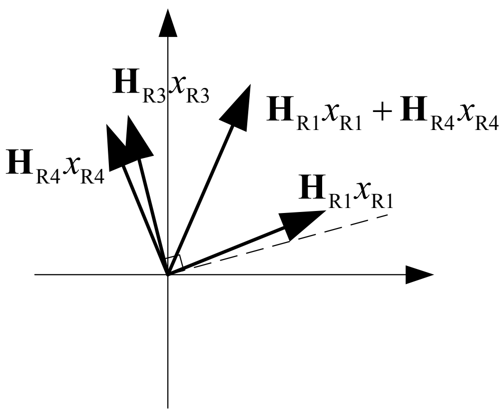

Figure 3.22: Case 3: Receive signal space

CHAPTER 4

Application of mutual information metric in multi-user scheduling

4.1 Introduction to multi-user grouping for MAC

Space-Division Multiple Access (SDMA) of multiuser MIMO systems allows multiple users to share the spatial domain simultaneously. This technique is able to offer a substantial gain in spectral efficiency and system throughput due to the fact that more than one user can be served using the same resource block (RB) in frequency and time.

Let us consider that the base station is equipped with multiple antennas and each user terminal has a single antenna. If the CSI of all the users is known at the base station, it would be possible to serve multiple users concurrently in the same time-frequency resource. By appropriately choosing the orthogonal users combined in a user group, information of different users in the same group can be spatially multiplexed and each group as a whole are coordinated using conventional scheduling methods, as introduced in Section 1.3. Therefore, system throughput can be improved and spectral efficiency can be increased.

However, if the channels of different users in a group overlap, SDMA can even lead to sum rate losses. Hence, The UEs with correlated channels should be coordinated to different SDMA groups, which are multiplexed on different resources in time or frequency.

Thus, the SDMA grouping algorithm must be able to measure the spatial compatibility of different users, and then determine if they can share the same spatial resource. Many algorithms have been proposed to find appropriate elements of a group. In [15], [16] and [25], Determinant pairing scheduling (DPS) and random pairing scheduling (RPS) are proposed.

DPS aims to maximize MIMO capacity based on channel condition numbers. However, this grouping scheme is not so accurate to achieve the maximum throughput. For one reason, channel capacity for virtual MIMO channels is just the upper bound of system throughput using joint decoding. The real transmission rate has a large gap compared with this upper bound. For the other reason, DPS is the approximation of channel capacity at high SNRs, so this may lead to a even larger gap at low SNR. RPS randomly selects users, and low computation complexity and overhead are obtained. It supports the users with high velocity motion but no separability of the users can be guaranteed.

In this chapter, I propose a user scheduling scheme based on mutual information metric. The scheme improves the throughput by employing a two-step scheme which picks up the primary user by round-robin scheduling in the first step and then invite the pair user which is able to maximize the performance metric. The simulation shows that the proposed strategy achieves almost the same system throughput performance as the optimal grouper and maintains a low computation complexity.

4.2 System model

Let us consider that the uplink multiuser MIMO systems consist of K users, transmitting to a receiver, i.e. BS, with N_r antennas. At each time, P active users out of total K users are selected to form a virtual MIMO group, where P is a variable, determined by the user grouping scheme. The P users in a group share the same frequency-time resource using SDMA. The receive signal at the BS is given by

$$\mathbf{y} = \sum_{i=1}^{P} \mathbf{H}_i \mathbf{x}_i + \mathbf{n} \quad (4.1)$$

$$\mathbf{y} = \tilde{\mathbf{H}}\tilde{\mathbf{x}} + \mathbf{n}, \quad (4.2)$$

where $\mathbf{y} \in \mathcal{C}^{N_r \times 1}$ is the receive signal vector at BS. $\mathbf{H}_i \in \mathcal{C}^{N_r \times N_t}$ denotes the channel matrix of the ith user, and $\mathbf{n} \sim \mathcal{CN}(0, \sigma_N^2 \mathbf{I})$ is complex symmetric white Gaussian noise. Assume that the transmitted symbols are uncorrelated and have unit variance, i.e., $\mathrm{E}\left\{\mathbf{x}_\mathrm{i}\mathbf{x}_\mathrm{i}^\mathrm{H}\right\} = \mathbf{I}$, $i \in \{1, \ldots, K\}$. The full channel matrix $\tilde{\mathbf{H}}$ of the Virtual MIMO can be represented by stacking of the channel matrices as

$$\tilde{\mathbf{H}} = [\mathbf{H}_1 \mathbf{H}_2 \cdots \mathbf{H}_P]. \quad (4.3)$$

The symbol vector $\tilde{\mathbf{x}}$ of all P antennas is given by

$$\tilde{\mathbf{x}} = [\mathbf{x}_1 \mathbf{x}_2 \cdots \mathbf{x}_P]^\mathrm{T}. \quad (4.4)$$

Furthermore, let us assume Gaussian signalling at all transmitters, perfect channel state information at the receivers, and *independent* decoding (alway treating signals of other users as noise). The total expected mutual information of the P user group is given by

$$\begin{aligned} I_{\text{total}} &= \sum_{i=1}^{P} I\left(\mathbf{x}_i; \mathbf{y}_i | \mathbf{H}\right) \qquad (4.5) \\ &= \sum_{i=1}^{P} \mathrm{E}\left\{ \log_2 \det\left[\mathbf{I} + \mathbf{H}_i \mathbf{H}_i^{\mathrm{H}} \left(\sum_{j=1, j\neq i}^{P} \mathbf{H}_j \mathbf{H}_j^{\mathrm{H}} + \sigma^2 \mathbf{I} \right)^{-1} \right] \right\}. \end{aligned}$$

To achieve the maximum mutual information, the finding of the optimal users should be able to maximize I_{total}. The optimal solution is assuredly found by exhaustively searching the solution space of all possible groupings. However, the complexity will increase exponentially with number of users and can get to an unacceptable complexity even for a moderate number of users. Therefore, sub-optimal scheduling algorithms that are able to find an efficient SDMA group with lower complexity are desired.

4.3 Grouping strategy

In order to design efficient grouping algorithms, two relevant aspects should be properly designed with acceptable complexity:

1. To avoid exhaustive search, a scheduling algorithm is required. It finds the SDMA group that maximizes (or minimizes) the performance metric without needing to compare all the possible combinations.

2. A performance metric with low complexity is needed in order to determine whether the users can be in the same SDMA group and to compare the performance of different groups.

4.3.1 Multi-user scheduling

The scheduling algorithm directly affects the performance in the multiuser scheduling. In this thesis, a two-step scheduling algorithm is considered. First, the scheduler periodically selects one user as primary user according to the round-robin scheduling approach and then selects another invited user to join the same resource block according to the value of the performance metric. This approach provides a suboptimal solution to the exhaustive search, however, it will greatly reduce the complexity of the pairing scheduling. Furthermore, this scheduling algorithm guarantees that each user is able to transmit at least once over K resource blocks, where K is the total number of users. Fig. 4.1 shows the principle of grouping 2 users out of total

6 users. Although individual user in a group may experience slightly lower throughput, a gain of the throughput per RB is achieved.

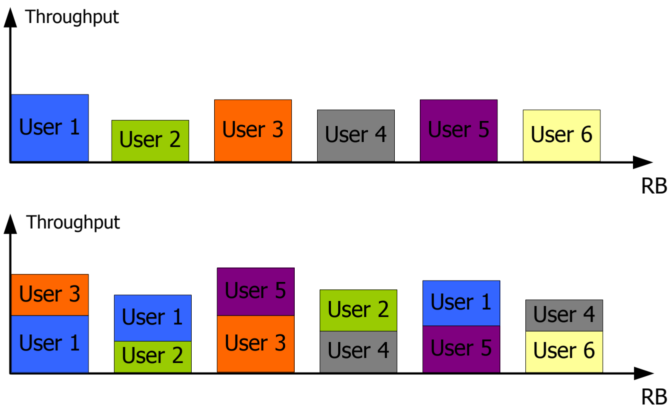

Figure 4.1: Example of grouping 2 users out of total 6 users

4.3.2 Grouping criteria

When the users in a SDMA group transmit data simultaneously, the interference will be unavoidable, which influences the system performance. The goal of the performance metric is to find the best user pairs for SDMA transmission with the least mutual impairment. Furthermore, the metric should be able to quantify the efficiency of the transmission to the i-th user when this user is spatially multiplexed in the same resource block with users j.

In this section, both channel orthogonality and system capacity are considered based on the mutual information metric. According to the objective function in (4.6), a metric aiming to maximize J is given by

$$J_{\text{total}} = \sum_{i=1}^{P} J\left(\mathbf{R}_i, \sum_{j=1, j\neq i}^{P} \mathbf{R}_j\right) \tag{4.6}$$

$$= \sum_{i=1}^{P} \log_2 \det\left(\mathbf{I} + \mathbf{R}_i \left(\sum_{j=1, j\neq i}^{P} \mathbf{R}_j + \sigma^2 \mathbf{I}\right)^{-1}\right) \tag{4.7}$$

where $\mathbf{R}$ is the $N_r \times N_r$ correlation matrix at the receiver and $\mathbf{R}_i = \mathrm{E}\left\{\mathbf{H}_i\mathbf{H}_i^{\mathrm{H}}\right\}$, $\mathbf{R}_j = \mathrm{E}\left\{\mathbf{H}_j\mathbf{H}_j^{\mathrm{H}}\right\}$. This metric improves the system performance by selecting the pair user that maximizes J_{total}.

In a SDMA group, it is known that if channels of the users are spatially orthogonal, the gain of system throughput can be obtained. Motivated by this, the scaled mutual information metric $\tilde{J}$, denoted as SMIM, is considered as another alternative metric, which is given by

$$\tilde{J}(\mathbf{R}_0, \mathbf{R}_\mathrm{I}) = \frac{J(\mathbf{R}_0, \mathbf{R}_\mathrm{I}) - J_{\min}(\mathbf{R}_0, \mathbf{\Gamma})}{J_{\max}(\mathbf{R}_0, \mathbf{\Gamma}) - J_{\min}(\mathbf{R}_0, \mathbf{\Gamma})}, \tag{4.8}$$

where $\tilde{J} \in [0, 1]$. More details about $\tilde{J}$ can be found in Section 2.2.1. A better channel orthogonality factor indicates a better eigenspace alignment between the users. As $\tilde{J}$ only takes small scale fading into account, it is insensitive to the change of signal to interferences power ratio. Therefore, this metric is able to provide the same opportunity for the cell edge users to be selected to transmit with the primary user.

For the multiuser scheduling in wireless system, there always exists a tradeoff between the user fairness and the system throughput performance. In order to maintain the fairness of individual user, a rate constraint $\alpha \cdot J_\mathrm{thr}$ for the primary user is introduced to cooperate with the metric, where

$$J_\mathrm{thr} = N_r \cdot \log_2(1 + \mathrm{SNR}) \tag{4.9}$$

is the maximum achievable value of mutual information metric at a certain SNR, by allocating the transmitted power equally to each eigenchannel. By adjusting α, a tradeoff between throughput and fairness can be achieved and the groupings only can be granted when the mutual information metric of the primary user i fulfills

$$J\left(\mathbf{R}_i, \sum_{j=1, j\neq i}^{P} \mathbf{R}_j\right) \geq \alpha \cdot J_\mathrm{thr}. \tag{4.10}$$

If no candidates satisfies J_thr, the primary user will transmit without any invited users. Since J of the primary user has been stored from the calculation of performance metric, using this criterion only slightly increases the computation complexity.

4.4 Algorithm comparison and simulations

In this section, the performance of DPS, RPS, conventional single user scheduling and our proposed SDMA grouping algorithms, i.e., MIM and SMIM will be evaluated by simulations. As in the practical multi-user MIMO systems [26], the common antenna configuration at base station is 2 or 4, in order to guarantee enough spatial separability, we consider a pair of concurrent users in the following simulations.

4.4.1 Review of other metrics

DPS considers the multi-user MIMO systems as a whole and selects the pairing user based on an interpolation of capacity maximization criterion.

The capacity of deterministic MIMO channel is known as

$$C = \log_2 \det(\mathbf{I} + \mathrm{SNR} \cdot \tilde{\mathbf{H}}\tilde{\mathbf{H}}^{\mathrm{H}}), \tag{4.11}$$

where $\tilde{\mathbf{H}}$ is the full channel matrix in (4.2). At very high SNRs, channel capacity can be approximated to

$$C = \log_2 \det(\tilde{\mathbf{H}}\tilde{\mathbf{H}}^{\mathrm{H}}) + \log_2(\mathrm{SNR}). \tag{4.12}$$

Then DPS is formulated as

$$D = \frac{\det(\tilde{\mathbf{H}}\tilde{\mathbf{H}}^{\mathrm{H}})}{\mathrm{tr}(\tilde{\mathbf{H}}\tilde{\mathbf{H}}^{\mathrm{H}})} \tag{4.13}$$

RPS selects the first user according to round-robin, and pick up the second one randomly. For making comparison, we also simulate the conventional scheduling without SDMA, named as 'single user'. The optimal grouping using (4.6), which posses an upper bound, is simulated as well.

4.4.2 Simulations

The simulations are performed for the uplink multi-access channels including 20 users with 2 antennas each and a BS with 2 antennas. The channel state information is assumed perfectly known at the receiver. In LTE system, power control in uplink is used to combat the power fluctuations due to path loss and shadow fading. In the following simulations, path loss and shadow fading are considered to be ideally compensated by power control and only small scale fading is considered. Therefore, the channel matrix of i-th user is defined as i.i.d channel with receive correlation matrices, i.e.,

$$\mathbf{H}_i \quad = \quad \mathbf{R}_i^{1/2}\mathbf{G}_i, \tag{4.14}$$

where $\mathbf{G}_i$ is $N_r \times N_t$ matrix with independent entries drawn from $\mathcal{CN}(0, 1)$. $\mathbf{R}_i \in 2\times 2$ is generated based on the eigenvalue decompositions $\mathbf{U\Lambda U}^{\mathrm{H}}$. The matrices $\mathbf{U}$ is uniformly chosen from the set of unitary matrices. The eigenvalue profile $\mathbf{\Lambda}$ is drawn from an exponential distribution with normalized mean $\mathrm{SNR}\cdot\sigma^2$. 1000 channel realizations are generated for each user and the receiver correlation is assumed unchanged within this time. Furthermore, I defined that all users are served once as primary user as a round and a total 100 rounds are simulated. The scheduling is performed at the beginning of each round.

Fig. 4.2 shows the CDF of average mutual information of the system at 0 dB receive SNR. Different constraints α are used to guarantee the transmission of the primary user and a large α is more likely to force the primary user occupies the whole resource block without sharing with other users. It can be observed that the average mutual information increases greatly using SDMA. Even for RPS, which offers the lowest gain in all the grouping schemes, the increase of system throughput is still considerable. The proposed strategy MIM has almost the same performance as the optimal one, which maximizes the expected mutual information. There is small throughput loss of DPS and SMIM compared with the optimal one.

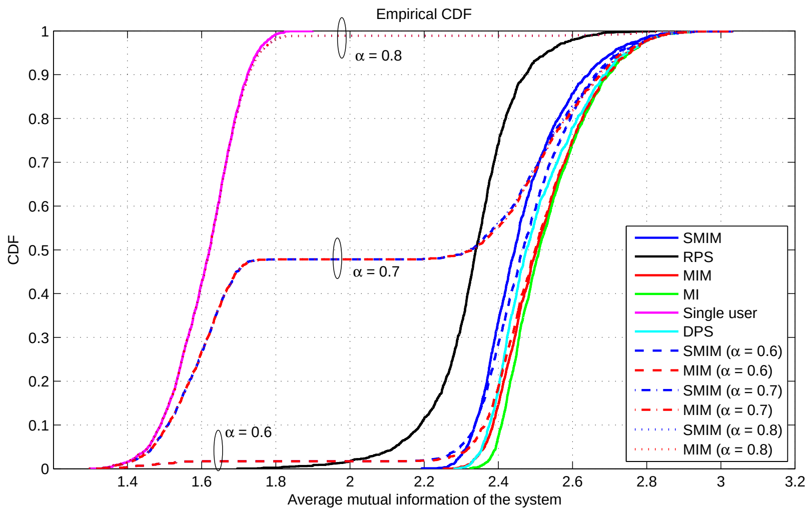

Figure 4.2: CDF of average mutual information of the system at 0 dB

In Fig. 4.3, the average mutual information using different transmission mode at different receive SNRs are plotted. The proposed algorithm offers around 3 dB gain over single user scheduling at 0dB and the gain of SDMA degrades as increase of SNR. From the figure, it can be observed that the SNR range of interest for SDMA is below 15 dB. Among all grouping schemes, The proposed strategy MIM outperforms DPS and almost coincides with the upper bound, i.e. MI. In the overloaded MIMO systems, i.e., total transmit antennas more than receive antennas, interference will inevitably exist. The advantage of MIM is that it is able to measure the quality of a grouping taking interference into account. However, DPS only treats the multiple users as a whole without considering interference between them.

Fig. 4.4 plots the average mutual information at different number of users for different transmission modes at 0 dB. Generally, more candidates provide more pairing choices, which benefits average throughput of the system. On the other hand, less number of users reduces the complexity of calculation and coordination. It can be observed that the performance of RPS remains unchanged since the channel state information is not taken into account. For other SDMA schemes, the averages mutual information increases with the number of users and for scenarios of more than 10 users, the improvement by increasing the number of users becomes very slight. Therefore, a total

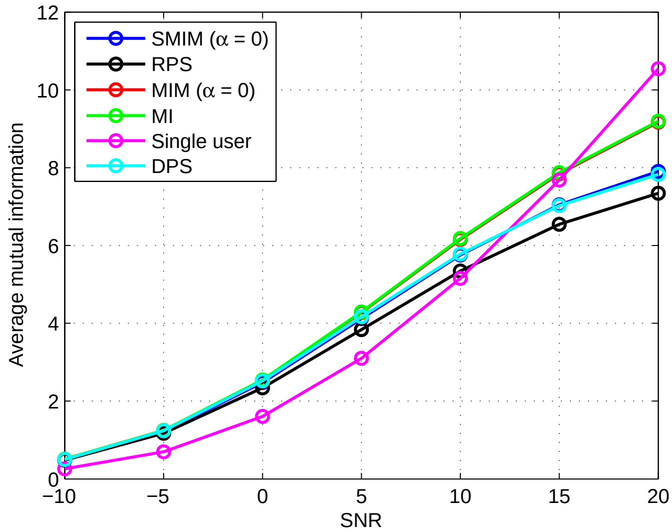

Figure 4.3: System average mutual information over different SNRs

$10-20$ users is a reasonable choice.

In Fig. 4.5, the average mutual information per user is given. Four subplots are simulated under 4 different α values. When $\alpha = 0$, no constraint is specified. The throughput is maximized at the cost of making a number of users suffer low rate. With the increase of α, less users transmit at low rate while on the other hand the number of high rate users is reduced as well. The CDFs of different SDMA schemes tend to coincide with the CDF of single user scheduling due to more users are restrained to transmit alone. It also can be observed that the CDFs are not smooth and the mutual information is likely to exhibit at some certain levels. The distributions of users at each level is determined by the number of times users transmit.

The previous simulation is performed when $N_{\mathrm{t}} = 2$. It is shown in [27] that reducing the number of streams transmitted by all users can provide benefits for system mutual information. Actually in a $N_{\mathrm{r}} = N_{\mathrm{t}} = P = 2$ system, if all users use a single stream, the mutual information of the system is often higher than if all users use the maximum possible number of streams [28], which is two in our case.

Similarly, by transmitting less number of streams in an uplink SDMA group, the mutual information of the system will also be increased. When $N_{\mathrm{t}} = 1$, each user just transmits using one eigenchannel. We regenerate the channel matrix in (4.14) by using a 2×1 $\mathbf{G}_i$ instead and each user is transmitting using only one transmit antenna. The average mutual information using different transmission mode at different receive SNRs are plotted in Fig. 4.6. Compared to the case with 2 transmit antennas, it is found

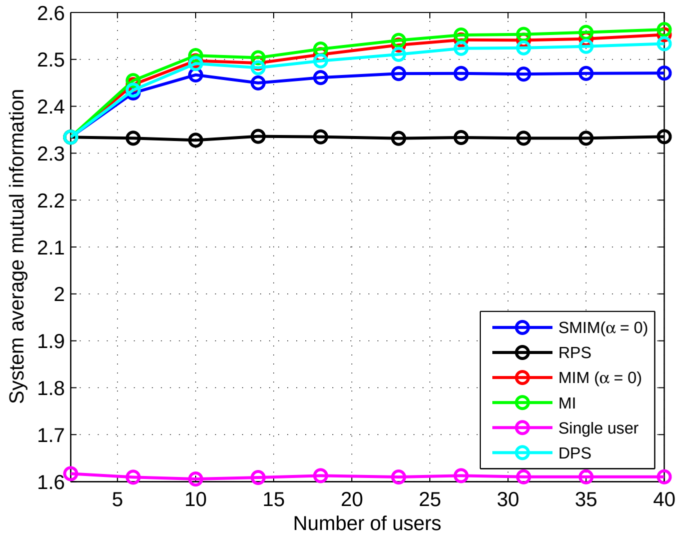

Figure 4.4: System average mutual information at different number of users

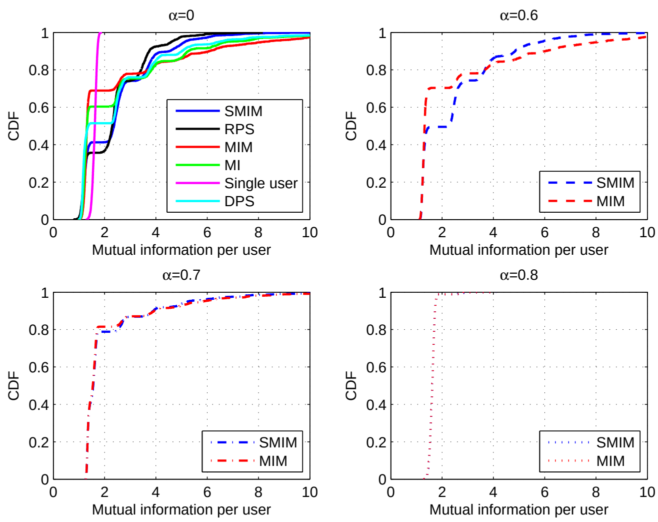

Figure 4.5: CDF of average mutual information per user

that system average mutual information increases greatly at high SNRs, i.e., above 15 dB. DPS outperforms due to the reduced interference of each other. Fig. 4.7 shows the CDF of average mutual information of the system at 0 dB with $N_t = 1$. Similarly, a higher α will make the more primary users occupy the whole resource block without sharing with other users.

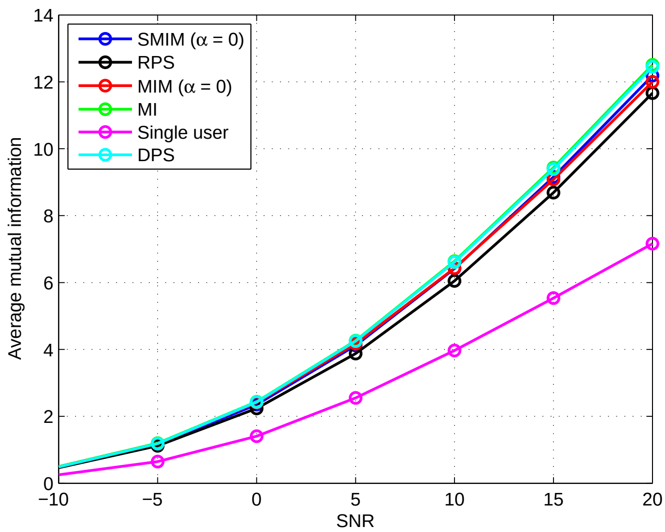

Figure 4.6: System average mutual information over different receive SNRs with $N_{\mathrm{t}} = 1$

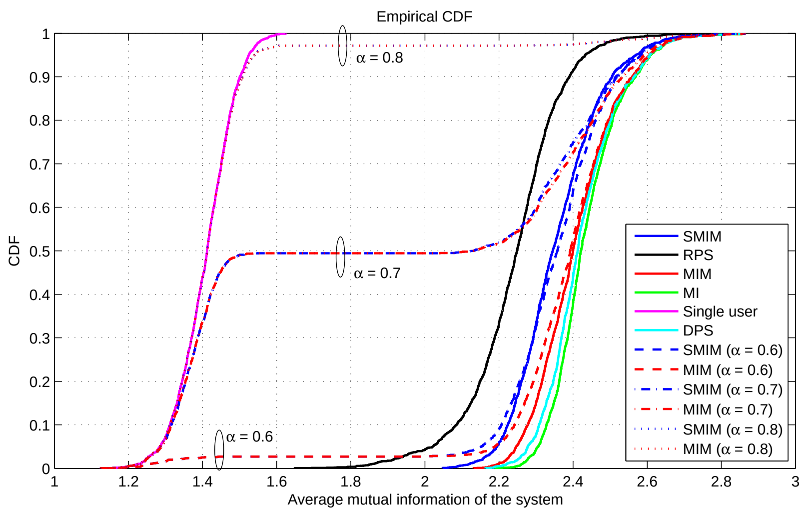

Figure 4.7: CDF of average mutual information of the system at 0 dB with $N_{\mathrm{t}} = 1$

CHAPTER 5

Conclusions

The primary target of this thesis was to study the spatial interference by means of the channel receiver correlation matrices.

I parameterized the multi-user MIMO channel model using the experimental data of 2009 PUCCO radio measurement campaign. I found that in indoor-to-indoor scenarios, the spatial compatibility between signal and interference is strongly determined by the position of the receiver. Moving receiver will give uniform-like distributed scaled mutual information metric. Similar results are also found when a moving transmitter is close to a static receiver. For other cases with a static receiver, the spatial compatibility varies slightly. In indoor-to-outdoor scenarios, the correlation matrices of different users in the same building are similar.

I evaluated and parameterized the multi-user MIMO channel model from the aspect of mutual information increase, the relationship between the eigenvalue structures of the receiver correlation matrices and the increase of mutual information is evaluated and an explicit expression is given. We found that channels with unbalanced eigenvalue structure (rank deficient) have large mutual information increase from maximally non-aligned to fully aligned.

A relationship between the distribution of mutual information metric and capacity increase was found. A channel with a uniform-like distribution of scaled mutual information metric is more likely to have a small increase of mutual information.

I evaluated and parameterized the multi-user MIMO channel model under interference from multiple users. I found that the subspace similarity of the multiple interferences greatly influences the mutual information metric, thus orthogonal addressed interferences should be coordinated.

I designed a user grouping scheme for uplink multi-access channels using the mutual information metric. The scheme consists of a round robin scheduler and a grouping criterion building on the mutual information metric. Simulations showed that this grouping scheme offers a gain in spectral efficiency and system throughput in overloaded MIMO systems due to more efficient use of spatial resources.

The future work regarding the multi-user MIMO channel model could be as follows:

- Assuming channel state information at the receivers, the model can be extended to include transmit precoding by introducing the corresponding precoding matrix into the equation.
- Relating the model to propagation-based models (i.e. ray tracing model), we can analyze the behavior of the model by taking into account the exact position, orientation of individual user, and the electrical properties of the environment.

The future work concerning the multi-user scheduling scheme could be as follows:

- Improve the scheduling algorithm by employing more efficient scheduling methods, i.e. proportional fairness and tree-based scheduling, instead of round-robin.
- Simulate in real systems and include signal processing algorithms for interference-impaired MIMO channels, i.e., channel estimations for interfering channels, interference cancellation receiver based on the obtained correlation matrix.

APPENDIX A

Experimental Set-up

The modeling of a radio channel requires to accurately know the propagation of electromagnetic waves in the real world. In this section, we focus on the channel measurements of the PUCCO October 2009 radio measurement campaign, which followed the Stanford July 2008 measurement campaign. An 8×8 MIMO channel sounder (Elektrobit Propsound, see Section A.1.1) was used throughout the campaign to make measurements in Universite catholique de Louvain (UCL), Belgium.

The measurement campaign is intended to encompass two distinct scenarios:

- Indoor-to-Indoor (I2I) MIMO/virtual MIMO measurements with nodes (single or multiple antennas) located at different positions in an office building.
- Outdoor-to-Indoor (O2I) measurements with a base station (BS) broadcasting into an office building and a series of users, each being equipped with one or more antennas.

More details on the full campaign can be found in [29].

A.1 Equipment

A.1.1 Channel Sounder

The UCL/ULB Elektrobit Propsound CS channel sounder was used throughout the campaign. It is capable of measuring up to 8×8 MIMO channels with a maximum null-to-null bandwidth of 200MHz centered at a frequency of 3.8 GHz.

The sounder utilizes the switched-array principle demonstrated in Fig. A.1. Only one link between a specific Rx element and Tx element is measured at the same time (using only one transmitter and one receiver chain). The link to be measured is selected by the switches at the Tx and Rx sounding units. At one time, only one Tx element is active while the other Tx elements keep silent. The switch at the Rx side scans all 8 antennas from Rx1 to Rx8. Then, the switch on the Tx side shifts to the next Tx element. One cycle is done after the 8×8 MIMO channel is measured once. The time for measuring one complete MIMO matrix thus depends on the number of Tx and Rx antennas used as well as on the length of the channel sounding sequence.

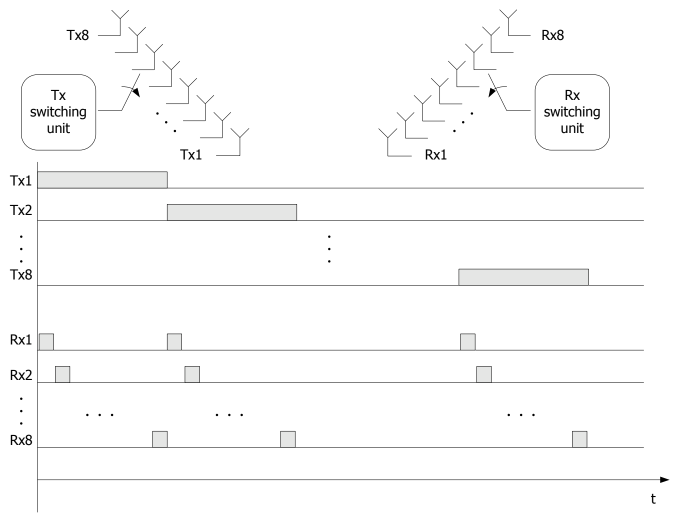

Figure A.1: Switched-array principle in one cycle

A.1.2 Antennas

The node antennas are highly efficient dipole antennas with an almost isotropic radiation pattern, with an antenna gain of 1.75 dBi. An array of dual-polarized patch antennas are used at the BS. The gain in the direction of the maximum radiation is 6 dBi.

A.2 Sounding parameters

The exact sounding parameters are provided in Table A.1. The burst mode was used, meaning that each 8×8 MIMO channel (i.e. one cycle) was measured in bursts of 4 cycles in order to increase SNR with a high cycle rate. From these values in the table, The number of bursts for one measurement is $1200/4 = 300$, the duration of one measurement was $300/2.65 = 113.2$s.

The recorded data of the channel transfer function is given by $\mathbf{H}[t, f, c]$, where t, f and c represents time index, frequency index and link index respectively. The total number of links is equal to $N_{\mathrm{Rx}} \times N_{\mathrm{Tx}}$, where N_{Rx} and N_{Tx} are the number of Rx antennas and the number of Tx antennas.

Table A.1: Sounding parameters

Parameters	I2I	O2I
Carrier frequency [GHz]	3.8	3.8
Transmit power [dBm]	23	23
Bandwidth [MHz]	50	50
No. Tx antennas	8	4
No. Rx antennas	8	8
Effective burst rate [Hz]	2.65	2.65
Burst length (No. cycles/burst)	4	4
Channel rate (within a burst) [Hz]	21.203	21.203
Code length (No. chips)	2047	4095
No. samples/chip	2	4
Measurement length (No. measured cycles)	1200	1200

A.3 Indoor-to-Indoor (I2I) Measurements

There are two kinds of scenarios: static and mobile. Static antenna scenarios were facilitated by attaching the antennas to desks, while mobile antenna scenarios were realized such that the antennas were handled by people in order to replicate realistic user motion. The antennas were connected to the switching unit via long low-loss RF cables. Each of the scenarios was carried out twice to collect more data and get rid of the artifacts.

In this thesis, we investigated the cases where each node was equipped with multiple antennas. Thus, the 8 nodes scenarios will be introduced in detail in the following. For 8 users, the scenarios investigated were:

- all 8 nodes were static with no people in the area,
- 4 nodes were moving locally over a small range (fixed feet) and 4 nodes were static,
- 4 nodes were moving over a larger range and 4 nodes were static,

The particulars of this scenarios is summarized by Fig. A.2.

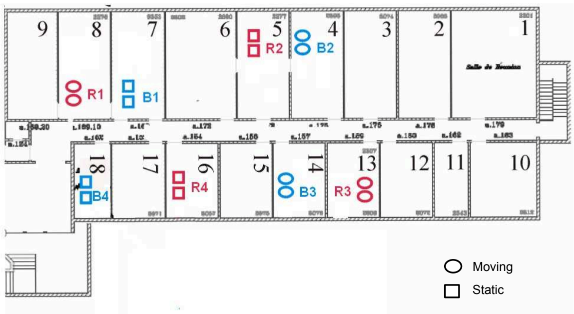

Figure A.2: Map of 8 nodes I2I distributed scenarios

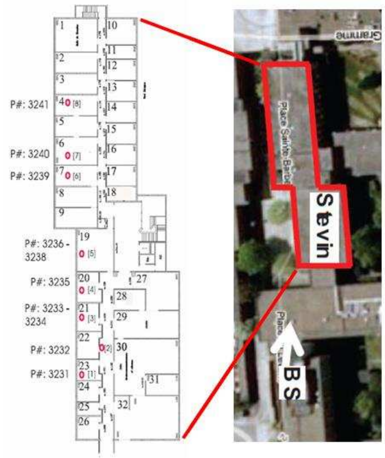

Figure A.3: Outdoor environment and 8 nodes I2O distributed scenario

A.4 Outdoor-to-Indoor (O2I) Measurements

A.4.1 Measurement setup and practice

Two different types of antennas were used for O2I measurements. Each user again employed omnidirectional dipole antennas connected to the Rx switching box. At the BS, 2 dual-polarized patch antennas (see Section A.1.2) were employed, giving a total of 4 antennas. These antennas were connected to the switching unit by means of short low loss RF cables. The BS was mounted on the top floor of the neighboring building broadcasting to the Stevin building (see Fig. A.3). These units required clock synchronization using a Rubidium reference since they were not in close proximity.

A.4.2 Scenarios

In O2I case, users were located in both the east and west wings. The following two scenarios were investigated:

- all nodes were moving locally over a small range (with fixed feet),
- all nodes were moving locally over a larger range.

A.5 Estimation of channel correlation matrices

For static measurements, the channel is stationary over time, and all frequency realizations are used to estimate the correlation matrices. This yields

$$\mathbf{R} = \sum_{t=1}^{T} \sum_{f=1}^{F} \mathbf{H}^{\mathrm{H}}(f,t)\mathbf{H}(f,t) \tag{A.1}$$

where $\mathbf{H}$ is a matrix of channel transfer function with size $N \times M$. N and M are the number of Rx antennas and the number of Tx antennas respectively. $\mathbf{R}$ is a $N \times N$ correlation matrix.

For mobile environment, receive correlation matrices were estimated from the data using a moving window in time:

$$\mathbf{R}(t) = \sum_{t'=t-T_{av}/2}^{t+T_{av}/2-1} \sum_{f=1}^{F} \mathbf{H}^{\mathrm{H}}(f,t')\mathbf{H}(f,t') \tag{A.2}$$

where $T_{av} = 20$. The channel is assumed to be stationary within T_{av}.

Bibliography

[1] A. J. Paulraj, D. A. Gore, R. U. Nabar, and H. Bölcskei, "An overview of MIMO communications — a key to gigabit wireless," *Proceedings of the IEEE*, vol. 92, pp. 198–218, February 2004.

[2] D. Gesbert, M. Shafi, D. Shiu, P. J. Smith, and A. Naguib, "From theory to practice: an overview of MIMO space-time coded wireless systems," *IEEE J. Select. Areas Commun.*, vol. 21, no. 3, pp. 281–302, 2003.

[3] G. Foschini and M. Gans, "On limits of wireless communications in fading environments when using multiple antennas," *Wireless Personal Communications*, vol. 6, pp. 311–335, 1998.

[4] S. M. Alamouti, "A simple transmit diversity technique for wireless communications," *IEEE J. Select. Areas Commun.*, vol. 16, no. 8, pp. 1451–1458, 1998.

[5] A. Nosratinia, T. E. Hunter, and A. Hedayat, "Cooperative communication in wireless networks," *IEEE Commun. Mag.*, vol. 42, no. 10, pp. 74–80, 2004.

[6] M. Dohler and Y. Li, *Cooperative Communications: Hardware, Channel and PHY.* Wiley, 2010.

[7] D.-S. Shiu, G. Foschini, M. Gans, and J. Kahn, "Fading correlation and its effect on the capacity of multielement antenna systems," *IEEE Transactions on Communications*, vol. 48, pp. 502–513, March 2000.

[8] N. Czink, B. Bandemer, C. Oestges, T. Zemen, and A. Paulraj, "Analytic multi-user MIMO channel modeling: Subspace alignment matters!," *submitted to IEEE Transactions of Wireless Communications*, 2011.

[9] J. Schiller, *Mobile Communications.* Addisson Wesley, 2003.

[10] S. Catreux, P. F. Driessen, and L. J. Greenstein, “Simulation results for an interference-limited multiple-input multiple-output cellular system,” *IEEE Commun. Lett.*, vol. 4, no. 11, pp. 334–336, 2000.

[11] R. Blum, “MIMO capacity with interference,” *IEEE Journal on Selected Areas in Communications*, vol. 21, no. 5, pp. 793–801, 2003.

[12] R. Janaswamy, *Radiowave Propagation and Smart Antennas for Wireless Communications.* Norwell, MA, USA: Kluwer Academic Publishers, 2001.

[13] J.-S. Jiang, M. Demirkol, and M. Ingram, “Measured capacities at 5.8 GHz of indoor MIMO systems with MIMO interference,” in *Vehicular Technology Conference, 2003. VTC 2003-Fall. 2003 IEEE 58th*, vol. 1, pp. 388–393 Vol.1, 2003.

[14] H. Wu, T. Haustein, and V. Venkatasubramanian, “Adaptive SIMO and SDMA transmission mode for single carrier FDMA uplink,” in *Proc. IEEE 19th Int. Symp. Personal, Indoor and Mobile Radio Communications PIMRC 2008*, pp. 1–5, 2008.

[15] Nortel, *UL Virtual MIMO Transmission for E-UTRA.* 3GPP, San Diego, USA, Oct. 2005.

[16] Nortel, *UL Virtual MIMO System Level Performance Evaluation for E-UTRA.* 3GPP, Seoul, Korea, Nov. 2005.

[17] N. Czink, B. Bandemer, C. Oestges, T. Zemen, and A. Paulraj, “Subspace modeling of multi-user MIMO channels,” in *IEEE VTC Fall 2011*, (San Francisco, USA), Sept. 2011.

[18] M. Herdin, N. Czink, H. Ozcelik, and E. Bonek, “Correlation matrix distance, a meaningful measure for evaluation of non-stationary MIMO channels,” in *IEEE VTC Spring 2005*, vol. 1, pp. 136–140 Vol. 1, 2005.

[19] M. Talih, “Geodesic Markov chains on covariance matrices,” tech. rep., Statistical and Applied Mathematical Sciences Institute, Mar. 2007.

[20] D. Sacristan-Murga and A. Pascual-Iserte, “Differential feedback of MIMO channel Gram matrices based on geodesic curves,” *IEEE Trans. Wireless Commun.*, vol. 9, no. 12, pp. 3714–3727, 2010.

[21] S. Helgason, *Differential Geometry, Lie Groups, and Symmetric Spaces.* American Mathematical Society, Providence RI, 2001.

[22] S. Fiori and T. Tanaka, “An algorithm to compute averages on matrix Lie groups,” *IEEE Trans. Signal Processing*, vol. 57, no. 12, pp. 4734–4743, 2009.

[23] B. Bandemer, “Choosing unitary paths,” tech. rep., Department of Electrical Engineering, Stanford University, 2010.

[24] R. W. Hamming, *Numerical Methods for Scientists and Engineers.* Dover Publications, 1987.

[25] Nortel, *UL MU-MIMO Performance Improvement for E-UTRA*. 3GPP, Orlando, FL USA, June 2007.

[26] D. Astely, E. Dahlman, A. Furuskar, Y. Jading, M. Lindstrom, and S. Parkvall, “LTE: the evolution of mobile broadband,” *IEEE Commun. Mag.*, vol. 47, no. 4, pp. 44–51, 2009.

[27] M. F. Demirkol and M. A. Ingram, “Control using capacity constraints for interfering MIMO links,” in *Proc. 13th IEEE Int Personal, Indoor and Mobile Radio Communications Symp*, vol. 3, pp. 1032–1036, 2002.

[28] R. S. Blum, J. H. Winters, and N. R. Sollenberger, “On the capacity of cellular systems with MIMO,” *IEEE Commun. Lett.*, vol. 6, no. 6, pp. 242–244, 2002.

[29] P. Chambers, P. Castiglione, L. Liu, F. Mani, F. Quitin, O. Renaudin, F. Sanchez-Gonzales, N. Czink, and C. Oestges, “PUCCO radio measurement campaign,” Tech. Rep. TD(10)11015, COST 2100 Temporary Document, Aalborg, Denmark, June 2-4 2010.